A MACROMOLECULAR NETWORK MODEL FOR COAL FLUIDITY

P.R. Solomon, P.E. Best*, Z.Z. Yu, and G.V. Deshpande
Advanced Fuel Research, Inc. 87 Church Street, East Hartford, CT 06108

ABSTRACT

We have developed a model for coal fluidity based on the decomposition and condensation of the macromolecular network under the influence of bond breaking and crosslinking reactions. The model is an extension of the FG-DVC model of coal pyrolysis. It employs a macromolecular network consisting of aromatic ring clusters linked by bridges. In the FG-DVC model, bond scissions are described by a single first order reaction with a distribution of activation energies, and crosslinking is related to CO_2 and CH_4 formation. The FG-DVC model predicts the yield of liquids produced during heating of the coal. The fluidity is dependent on the relative amounts of the liquid, (molecules detached from the network) and solid (the remaining network) and on the fluidity of the liquid component. The fluidity of the liquid component depends on the average molecular weight of the liquid and on the temperature. Excellent agreement has been obtained between the model predictions for fluidity and low temperature fluidity measurements of Oxley and Pitt, Fitzgerald and van Krevelen. Good agreement has been obtained at high temperatures between the model predictions and measurements of Fong for the onset of the fluidity and the peak fluidity value. The loss of fluidity, however, is predicted to occur sooner than is indicated by the data. The data covers over four orders of magnitude in fluidity and four coals with carbon concentration between 80 and 90%.

INTRODUCTION

When bituminous coals are heated, they can decompose sufficiently to become liquid. Those in the range of 82 to 89% carbon achieve the highest fluidity (1,2), but even lignites, if heated rapidly enough can exhibit some fluidity (3). The understanding and ability to predict a coal's fluid properties is important in many processes. In liquefaction, highly fluid coals dissolve quickly in the process solvent so that further chemistry occurs by liquid/liquid interactions while non-fluid coals must undergo slower solid/liquid interactions. In combustion or gasification, fluidity controls particle swelling (4), agglomeration of particles, char reactivity (5), and subsequent fragmentation (6) of char. In coke making, fluidity controls the coke properties (7,8). Fluidity also affects the growth of carbon fibers from coal tars.

There are a number of factors which contribute to the fluidity of coal liquid. They include: i) the fluidity of the liquid part itself, with and without molecular entanglements; ii) the dependence of this fluidity on temperature; iii) the contributions of suspended solids in the liquid, both "chunks" of char, and mineral particles; and iv) the formation of a foam due to trapped gases.

Several models for coal liquid viscosity have been proposed which consider all of the influences except the trapped gases. The models were based on the two step process described by van Krevelen and coworkers (1,9), which assume the following reactions to occur on heating.

$$\text{coal} \xrightarrow{\ k_1\ } \text{metaplast} \xrightarrow{\ k_2\ } \text{coke}$$

where k_1 and k_2 are reaction rate constants. In the viscosity models the change of fluidity is assumed to result only from the change in solids mass fraction, ϕ_s (coal and coke) in the melt. Thus Bronowski et al. (10) used an expression in which fluidity was directly proportional to the mass fraction $(1-\phi_s)$ of fluid (metaplast) present. Expanding on this, Fitzgerald (11,12) used an equation which described the relative fluidity as depending on fluid fraction raised to a power n (where n was chosen to be 2.5). This power law expression was based on earlier work by Roscoe (13) and Brinkman (14). In a similar manner, Fong et al. (15) used an expression put forward by Frankel and Acrivos (16), in which the fluidity also depends on a power of the fluid fraction. Their model has the

*University of Connecticut, Physics Department and Institute of Material Science, Storrs, CT 06268

extra feature of a critical solids-volume-fraction at which fluidity disappears. This critical value occurs at the maximum volume fraction that the solids can occupy as limited by particle-particle interaction. At this critical value, the liquid fraction is insufficient to separate the solid particles. Its value is 0.64 for randomly close-packed spheres, while it ranges from 0.5 to 0.9 for other systems, depending on particle shape and state of agglomeration (17). Viscosity models predict that the fluidity vanishes for volume fractions equal to or greater than the critical value, and we refer to this as the inhomogeneous gel point. The chosen critical value in Fong's model was at a volume fraction of unity, somewhat higher than usual (17). A similar model was used by Oh (18). The above models gave good fits to data, although in each case the model parameters (k_1, k_2, n and the critical solids volume fraction) were chosen to fit data from a particular coal studied in a limited number of experiments covering a narrow range of heating rates, or holding temperatures.

Based on the observation that coal can be considered as a macromolecular network to which theories of crosslinked polymers may be applied (1,2,19,25,26), we have examined the polymer literature of viscosity in polymer melts (17,27-32). For non-reacting melts of branched polymers at molecular sizes below those sufficiently large for entanglements, there is experimental and theoretical support for viscosities which depend exponentially on side-arm molecular mass (27). These same authors determined temperature-dependent activation energies for viscosity, for temperatures below 200°C. It is noted that at higher temperatures (~ 600 K) Nazem found temperature independent activation energies for the viscosity of carbonaceous mesophase pitch (28).

In reacting melts, the manner in which average molecular weight varies with extent of reaction in a homogeneous melt has been considered in the branching theory described by Macosko and coworkers (29). Insofar as it describes molecular weight distributions, this theory duplicates and extends the results of older combinatorial methods developed by Flory (30) and by Stockmayer (31). A particular result of Macosko's work is that measured viscosity correlates well with the weight average molecular weight of the largest linear path through the molecules. This theory predicts that the homogeneous gel-point (the point at which the viscosity goes to infinity) appears at the first occurrence of a solid phase.

It is not clear whether Macosko's approach is appropriate for coal and it has not been tested. Coal is typically an inhomogeneous reacting melt where the reaction coal ---> metaplast is the inverse of the polymerization, and metaplast ---> coke is an example of repolymerization and crosslinking. The inhomogeneities result from several factors including: starting with a powdered solid (which would be sufficient to insure inhomogeneity), having a material consisting of diverse maceral types, and containing mineral grains. Theories which describe the viscosity of a suspension of a solid in a liquid, such as those mentioned above for coal, are general in their application (17,32), and also apply to suspensions of a solid in a polymer melt.

We have employed polymer concepts to describe tar and extract formation in coal pyrolysis, initially employing linear chain statistics (33,34) and subsequently employing network statistics (35-38). Our "DVC" model includes the processes of **Depolymerization** (bond breaking), **Vaporization** (mass transport), and **Crosslinking**. This model was combined with our functional group (FG) model for gas evolution (4,39-41) to provide the general FG-DVC coal pyrolysis model in which the crosslinking process is related to the evolution of certain gas species (42,43). The FG-DVC model employs Monte Carlo methods to compute the network properties. More recently, network models of thermal decomposition have been proposed employing percolation theory (44,45). We have also employed percolation methods for the statistical calculations in the FG-DVC model (46).

The fluidity model presented here employs the FG-DVC model to predict the molecular weight distribution of the decomposing macromolecular network. From this distribution, a solid fraction ϕ_s and a liquid fraction with a weight-average molecular weight are defined. These parameters are employed using the concepts of inhomogeneous mixtures to predict the fluidity from the solid fraction, the liquid viscosity and the temperature (17,28,32). The model predictions are compared with measurements made with a Gieseler plastometer (1,47,48) and with the high temperature fluidity measurements of Fong et al. (15).

EXPERIMENTAL

The low temperature fluidity data employed in this paper is literature data obtained with a Gieseler plastometer. Descriptions of the apparatus and operation may be found in the literature (49,50). The viscosity is determined by measuring the rotation rate of a stirrer in the sample when constant torque is applied. There are many problems of translating stirrer rotation speed to viscosity in poise and most researchers simply report data in degrees/min or dial divisions/min (DDPM) where one DDPM = 3.6°/min. Some data of van Krevelen was reported in poise (1). We have used these data in conjunction with data for the same coal reported in degrees/min to obtain the calibration $1°/min = 0.7 \times 10^{-8}$ rhe's where 1 rhe = 1/poise.

In making fluidity measurements on coal, it has been found that there is an initial softening of coal on heating which is reversible, and has been associated with melting and hydrogen bond breaking. This is followed by a sharp rise in fluidity due to the decomposition of the macromolecular network due to covalent bond breaking, and it is from this point that our model seeks to describe the processes. This sharp rise is illustrated in Fig. 1 which presents the measured fluidity of a bituminous coal as a function of time as the coal was heated from 300°C at 3°C/min to 407°C and held at constant temperature (48). The slower fall in fluidity with time is due to crosslinking which resolidifies the network. This crosslinking rate is linearly correlated with the initial rate for the evolution of CH_4 (38,42,43,51).

The high temperature data was obtained by Fong et al. (15) in a device designed for rapid heating. Coal is contained in a pancake shaped cavity in which a disk driven at constant torque is allowed to rotate. The rotation speed was related to viscosity in poise using standards of known viscosity.

The model we present employs both the coal composition and the kinetic rates for bond breaking and gas evolution. The crosslinking rate is related to the gas evolution. Since it was not possible to obtain samples of the original coals used for the viscosity measurements we have selected from the Argonne coal sample collection, those which best match the reported coals in carbon concentration and volatile matter. Table I presents the available data on the coals whose viscosities have been measured and the Argonne coal used in the model. More complete composition data for the Argonne coals were presented by Voores (52). The previously determined kinetic rates and model parameters were presented by Serio et al. (41,53). A comparison of the weight loss at constant heating rate of the Argonne coals and the coals employed in the study of van Krevelen (1) is presented in Fig. 2.

THEORY

The theory of coal fluidity consists of two parts: i) a macromolecular network model (FG-DVC) to predict the liquid fraction and average molecular weight of the liquid as a function of time and temperature; and ii) empirical expressions to predict fluidity from the liquid fraction, the average molecular weight of the liquid and the temperature.

To predict the liquid fraction and its average molecular weight, we employ a model which describes the decomposition or condensation of the macromolecular network under the influence of bond breaking and crosslinking reactions (42,43). Our model employs a sample macromolecular network in the computer consisting of aromatic ring clusters (monomers) linked by bridges. The bridges are either broken by bond scission reactions or are formed by crosslinking. As discussed previously (38,42,51), crosslinking occurs at low temperatures for low rank coals by a process apparently associated with CO_2 evolution. Crosslinking at moderate temperatures occurs by a process associated with CH_4 evolution. It is this process which leads to the reduction of fluidity shown in Fig. 1. The chemical justification for the association of crosslinking with CH_4 evolution is that the CH_4 is released by an ipso-substitution reaction involving a free radical connected to a ring cluster. Other peripheral groups may also be released in a similar manner.

A simple example of the model is shown in Fig. 3. Figure 3a shows the starting molecule. As explained previously (42,43), the number of branch points (initial crosslinks) is chosen to match the expected molecular weight between crosslinks. The length of the linear chains ℓ which are crosslinked is selected so that the fraction of unattached small monomer clusters matches the

measured fraction of pyridine solubles. The position of the bonds is randomly chosen. The molecular weight distribution is shown in Fig. 3b. When bonds are broken, more small molecules are formed as shown in Fig. 3c and 3d.

As discussed below, the viscosity is related to the liquid fraction produced during the break up of the network. The liquid fraction consists of all molecules detached from the starting macromolecular network (the solid fraction). Operationally we count the largest 3 molecules as belonging to the solid fraction and all others as belonging to the liquid fraction. This is a convenient approximation which gives results that agree reasonably well with experiment and do not depend on the molecular weight of the starting computer molecule. We have also used just the largest molecule as the solid fraction and found that computed results are similar but nosier.

An important feature of a homogeneous network model is that the break-up or solidification of the network occurs near a homogeneous "gel point" where the number of unbroken bonds per ring cluster (monomer), α, reaches a sufficiently low value. This gel point for a polymerizing melt occurs at the first appearance of the solid (or in the case of a decomposing network when the liquid fraction goes to 1.0) since the solid in a homogeneous melt extends throughout the entire melt. For most network geometries the break-up of the network occurs between $\alpha = 1.0$ and $\alpha = 0.8$.

For an inhomogeneous melt (such as expected for a liquefying powdered coal sample), the solids can appear as isolated particles so the gel point occurs at a higher solid fraction (lower liquid fraction). Based on the inhomogeneous model of fluidity discussed below, the liquid fraction must only exceed 0.3 before appreciable fluidity can occur. With the network geometry assumed for this model, this minimum liquid fraction is achieved at a critical value α_c of 0.95. For bituminous coals, this critical value can be achieved in pyrolysis and the coal melts and becomes fluid. For low rank coals, the effects of low temperature crosslinking is to increase α so that in some cases the network cannot come apart by normal pyrolytic reactions. Figure 4 compares the variation in α with time at constant temperature for a lignite and a bituminous coal. Also shown are the individual contributions to the total bond count and resulting fraction of the network which becomes liquid. The value of α for the lignite has a sharp increase at low temperatures due to CO_2 related crosslinking. This can be seen by the appearance of CO_2 related bonds in Fig. 4d. These bonds are a significant fraction of the total bonds connecting the network. With this large number of additional bonds, the value of α never achieves the critical value ($\alpha_c = 0.95$) and the solid fraction of the coal remains too high to liquefy. On the other hand, α for the bituminous coal is not increased by CO_2 related crosslinking. The value of α falls below the critical value and sufficient liquid fraction is produced for the network to disintegrate and become fluid.

The viscosity model used here has terms that depend on the coal liquid temperature, the weight average molecular weight of the liquid fraction, and the volume fraction of solids, with an inhomogeneous gel-point. It is the last two factors which are most important.

In common with previous studies of coal viscosity a two-phase model is used. The particular equation chosen is that put forward by Mooney (17,32)

$$\ln (\eta/\eta_{liq}) = \frac{k_E \phi_s}{1 - \phi_s/\phi_c} \tag{1}$$

where η is the viscosity of the suspension, η_{liq} the viscosity of the liquid, k_E is the Einstein coefficient, and ϕ_s is the volume fraction of solids, having a critical value ϕ_c at which η goes to ∞. Values of the constants are listed below.

Based on the model by Bartels et al. (27), the viscosity of the liquid phase is given by

$$\eta_{liq} = C \exp (E_\eta/RT^*) \exp (M_w/M_e) \tag{2}$$

which on combining with Eq. 1 leads to

$$\eta = C \exp(E_\eta/RT^*) \exp(M_w/M_e) \exp\frac{k_E\,\phi_s}{1 - \phi_s/\phi_c} \tag{3}$$

The constants used in the viscosity theory are as follows:

C: proportionality constant, $C = 1.0 \times 10^{-24}$ Poise
k_E: Einstein coefficient, $k_E = 5.0$
E_η: Activation energy for viscosity, $E_\eta = 8 \times 10^4$ kcal/mole
M_e: Molecular weight parameter, $M_e = 1000$
ϕ_c: Volume fraction of the solid phase at the gel-point, $\phi_c = 0.7$
M_w: Weight average molecular weight of the liquid
T^*: Absolute temperature, cut-off at 708 K

i.e., $T^* = T$ for $T \le 708$ K: $T^* = 708$ for $T > 708$ K

The value of $k_E = 5$ was arrived at empirically , i.e., to fit the data. This value, however, matches the situation in which liquid is entrapped within large agglomerates of solid (54). The value of the activation energies for coal was chosen based on measured liquid viscosities (from 5×10^4 to 10×10^4 kcal/mole) determined by Waters (55). Waters also showed that coal liquid behaves as a Newtonian fluid at strain rates encountered in standard viscosity measurements. The use of a cut-off temperature was introduced by Nazem (28).

RESULTS

There are two aspects to validating the model by comparison with data. The first is that the FG-DVC model should provide good predictions for pyrolysis products; the second is the comparison of predictions to fluidity data. Extensive comparisons of the FG and FG-DVC models have been made by Solomon et al. (39,40,42,43) and Serio et al. (41,53). These comparisons show good agreement between theory and experiment using rank independent kinetics for the Argonne coals and several other coals. An example of the fit of methane evolution for pyrolysis at 30°C/min for several coals used in this study is presented in Fig. 5. There are some differences between the predicted and observed evolution curves (the observed evolution in high rank coals is slightly slower than predicted), but in general the agreement is good.

All the viscosity data were fitted using the same viscosity equations and same constants. The only variable was the kinetic rate for bond breaking and crosslinking. When fitting the viscosity data, it was found that the slight differences in methane evolution (which is related to moderate temperature crosslinking) and in tar evolution (which is related to the bond breaking rates) adversely affected the viscosity prediction. For the viscosity results, the bond breaking and methane rates were adjusted to match the slow heating rate evolution curves. An example of the new predictions for the Upper Freeport coal is presented in Fig. 6. The new rates are presented in Table I. One additional change was made in the FG-DVC model to better match the fluidity data. This was to increase the crosslinking efficiency for methane from 1 to 1.5 crosslinks formed per methane evolved. This improved the fits to the fluidity data and can be justified on the basis that the evolution of gases formed from other peripheral groups (ethane, propane, etc.) may also lead to crosslinking.

The first example of the application of the model to predict fluidity is shown in Fig. 7. The data is from Oxley and Pitt (47) obtained by heating during an 11 minute period to constant temperatures of 400, 420, and 440°C. The coal is believed to be similar to the Upper Freeport. The agreement is excellent in following the increase and decrease in fluidity due to bond breaking and crosslinking, and in fitting the two orders of magnitude change in fluidity over a 40°C change in temperature.

Results for a higher rank coal studied by van Krevelen at constant heating rates are presented in Fig. 8a. The coal composition picked to represent the coal was that of the Pocahontas. However, the fluidity maximum for the coal is lower than expected based on the weight loss curve for Pocahontas. The bond breaking rate for this coal was, therefore, picked to be higher than we would expect for the Pocahontas coal. The theoretical predictions in Fig. 8b are in excellent agreement with the data.

Results for a Pittsburgh Seam coal obtained at high heating rates by Fong et al. (15) are presented in Fig. 9 as the symbols. The theory is shown as the lines. There is good agreement between theory and experiment for the onset of fluidity and for the maximum fluidity. The loss of fluidity is, however, predicted to occur much sooner than expected. The extract yield obtained by Fong et al. (15) in a heated grid experiment is also shown as a dashed line. The disappearance of fluidity predicted by our model does, however, appear to coincide with the disappearance of the extract yield. This is as expected since the model is dependent on the liquid fraction. The fact that the fluidity and extract data do not agree, may suggest that there are differences in temperature between the two apparatuses.

A number of additional comparisons were made between theory and experiments. A summary of the predicted and measured maximum fluidities for all the cases is presented in Fig. 10. There is good agreement over a fluidity range of five orders of magnitude and a temperature range of several hundred degrees.

CONCLUSION

1) A model for fluidity of coal has been developed based on a macromolecular network concept.

2) The network model is used to predict the fraction of liquids and the average molecular weight of the liquids under the combined effects of bond breaking and crosslinking.

3) The empirical model for an inhomogeneous melt assumes the fluidity to depend on the liquid fraction in the melt, on the viscosity of the fluid and on the temperature.

4) Good agreement is obtained with data for four coals which covers five orders of magnitude in fluidity and several hundred degrees in temperature. This agreement is obtained with fixed parameters in the empirical fluidity equations but with adjustments of the bond breaking and crosslinking rates to better fit the pyrolysis product yields.

5) At this stage of the development, we have a model which works for a variety of data, but is not necessarily unique. Emphasis is currently being placed on extending the range of applicability and on optimizing the model assumptions and constants.

ACKNOWLEDGEMENT

REFERENCES

1. Van Krevelen, D.W., Coal, Elsevier, Amsterdam, (1961).
2. Sanada, Y. and Honda, H. Fuel, 45, 295, (1966).
3. Solomon, P.R., Serio, M.A., Carangelo, R.M., and Markham, J.R., Fuel, 65, 182, (1986).
4. Solomon, P.R. and Hamblen, D.G., in Chemistry of Coal Conversion, R.H. Schlosberg, Editor, Plenum Publishing, NY, Chapter 5, pp 121-251, (1985).
5. Serio, M.A., Solomon, P.R., Bassilakis, R., and Suuberg, E.M., ACS Div. of Fuel Chem. Preprints, 34, (1), 9, 1989.
6. Helble, J.J. and Sarofim, A.F., Combustion and Flame, 76, 183, (1989).
7. Marsh, H., Fuel, 52, 205, (1973).
8. Marsh, H. and Neavel, R.C., Fuel, 59, 511, (1980).
9. Chermin, H.A.G. and van Krevelen, D.W., Fuel, 36, 85, (1957).
10. Bronowski, J., Fitzgerald, D., Gillings, D.W., and Rhys-Jones, D.C., Nature, 171, 389, (1953).
11 Fitzgerald, D., Fuel, 35, 178, (1956).
12. Fitzgerald, D., Trans. Faraday Soc., 52, 362, (1956).
13. Roscoe, Brit. J. Appl. Phys., 3, 267, (1952).
14. Brinkman, J., J. Chem. Phys., 20, 571, (1952).
15. Fong, W.S., Khalil, Y.F., Peters, W.A., and Howard, J.B., Fuel, 65, 195, (1986).

16. Frankel, N.A., and Acrivos, A., Chem. Eng., Sci., **22**, 847, (1976).
17. Nielsen, L.E., Mechanical Properties of Polymers and Composites, Vol. 2, Marcel Dekker, Inc. NY, (1974).
18. Oh, M.S., "Softening Coal Pyrolysis", PH.D. Thesis, Massachusetts Institute of Technology, (1985).
19. Green, T.K., Kovac, J., and Larsen, J.W., Fuel, **63**, 935 (1984).
20. Green, T.K., Kovac, J., and Larsen, J.W., in "Coal Structure," R.A. Meyers, Ed., Academic Press, NY (1982).
21. Nelson, J.R., Fuel, **62**, 112, (1983).
22. Lucht, L.M. and Peppas, N.A., Fuel, **66**, 803, (1987).
23. Lucht, L.M., Larsen, J.M., and Peppas, N.A., Energy & Fuels, 1, 56, (1987).
24. Green, T., Kovac, J., Brenner, D., and Larsen, J., Coal Structure, (R.A. Meyers, Ed.), Academic, NY, p 199, (1982).
25. Hall, P.J., Marsh, H., and Thomas, K.M., Fuel, **67**, 863, (1988).
26. Hirsch, P.B., Proc. Roy. Soc., **A226**, 143, (1954).
27. Bartels, C.R., Crist, B., Felters, L.J., and Graessley, W.W., Macromolecules, 19, 785, (1986).
28. Nazem, F.F., Fuel, 59, 851, (1980).
29. Macosko, C.W., Brit. Polymer Journ., **17**, 239, (1985), and references therein.
30. Flory, P.J., J. Am. Chem. Soc., **63**, 3083, 3097, (1941); see also Principles of Polymer Chemistry, Cornell University Press, Ithaca, NY, Chapter 9, (1953).
31. Stockmayer, W.H., J. Chem. Phys., **11**, 45, (1943); also **12**, 125, (1944).
32. Mooney, M., J. Colloid Sci., **6**, 162, (1951).
33. Solomon, P.R. and King, H.H., Fuel, 63, 1302, (1984).
34. Squire, K.R., Carangelo, R.M., DiTaranto, M.B., and Solomon, P.R., Fuel, **65**, 833, (1986).
35. Squire, K.R., Solomon, P.R., DiTaranto, M.B., and Carangelo, R.M., ACS Div. of Fuel Chem. Preprints, **30**, (1), 386, (1985).
36. Solomon, P.R., Squire, K.R., and Carangelo, R.M., Proceedings of the Int. Conference on Coal Science, Sydney, Australia, p. 945, (1985).
37. Solomon, P.R. and Squire, K.R., ACS Div. of Fuel Chem. Preprints, **30**, (4), 347, (1985).
38. Solomon, P.R., Hamblen, D.G., Carangelo, R.M., Serio, M.A., and Deshpande, G.V., Combustion and Flame, **71**, 137, (1988).
39. Solomon, P.R., Hamblen, D.G., Carangelo, R.M., and Krause, J.L., 19th Symposium (Int) on Combustion, The Combustion Institute, Pittsburgh, PA, 1139, (1982).
40. Solomon, P.R., Coal Structure, Advances in Chemistry Series, 192, 95, (1981).
41. Serio, M.A., Hamblen, D.G., Markham, J.R., and Solomon, P.R., Energy and Fuel, **1**, 138, (1987).
42. Solomon, P.R., Hamblen, D.G., Carangelo, R.M., Serio, M.A. and Deshpande, G.V., Energy and Fuels, **2**, 405, (1988).
43. Solomon, P.R., Hamblen, D.G., Deshpande, G.V. and Serio, M.A., A General Model of Coal Devolatilization, Int. Coal Sci. Conf. The Netherlands, October 1987.
44. Niksa, S. and Kerstein, A.R., Fuel, 66, 1389, (1987).
45. Grant, D.M., Pugmire, R.J., Fletcher, T.H., and Kerstein, A.R., Energy & Fuels, 3, 175, (1989).
46. Solomon, P.R., Hamblen, D.G., and Yu, Z.Z., "Network Models of Coal Thermal Decomposition", ACS Div. of Fuel Chem., **34**, paper presented at this conference, (1989).
47. Oxley, G.R. and Pitt, G.J., Fuel, **37**, 19, (1958).
48. Fitzgerald, D., Fuel, **35**, 178, (1956).
49. Lowry, H.H., Chemistry of Coal Utilization, J. Wiley, NY, (1963).
50. ASTM D 2639-74 (reapproved, 1980).
51. Deshpande, G.V., Solomon, P.R., and Serio, M.A., ACS Div. of Fuel Chem. Preprints, **33**, (2), 310, (1988).
52. Voores, K., ACS Div. of Fuel Chem. Preprints, **32**, (4), 221, (1987).
53. Serio, M.A., Solomon, P.R., Yu, Z.Z., Deshpande, G.V., and Hamblen, D.G., ACS Div. of Fuel Chem. Preprints, **33**, (3), 91, (1988).
54. Lewis, T.B. and Nielsen, L.E., Trans. Soc. Rheol, **12**, 421, (1968).
55. Waters, P.L., Fuel, **41**, 3, (1962).

TABLE 1 - SUMMARY OF COAL PROPERTIES

EXPERIMENTS:	FITZGERALD	FONG	OXLEY & PITT	VAN KREVELEN
Volatile Matter	34.4%	41.7%	30.3%	24.0%
C %	N/A	83.2	N/A	N/A

COAL USED FOR MODELING	UPPER KNAWHA	PITTS NO. 8	UPPER FREEPORT	POCAHONTAS Composition[+]
Volatile Matter (MAF)	37.6%	41.7%	31.6%	19.5%
C% (MAF)	82.6	83.2	85.6	91.1
E_{bonds} (cal/mole)	59200	60000	62000	63000
A_{bonds}	5.08×10^{15}	8.57×10^{14}	3.08×10^{15}	7.0×10^{16}
σ_{bonds}	1500	1500	1500	1500
Bond Breaking Rate @ 450°C	8.43×10^{-3}	8.17×10^{-4}	7.37×10^{-4}	8.39×10^{-3}
E_{CH4-L} (cal/mole)	60000	60000	56000	60000
A_{CH4-L}	4.5×10^{13}	7.5×10^{13}	3.0×10^{12}	1.0×10^{13}
σ_{CH4-L}	1500	1500	1000	1800
$CH_4 - L$ Rate @ 450°C	4.29×10^{-5}	7.15×10^{-5}	4.55×10^{-5}	9.54×10^{-6}

N/A: Not Available

[+]Based on fluidity data, the van Krevelen coal (24% volatile) appears to have kinetic rates comparable to the 90% carbon coals in Fig. 2 rather than the Pocahontas coal. For this reason the kinetic rates in the Table are higher than expected for Pocahontas.
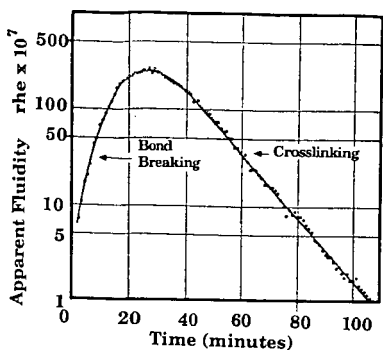
Figure 1. Apparent Fluidity as a Function of Time at 407°C for a Typical Coking Coal (34.4 percent dry ash free volatile matter, coal rank code number 401b). From Ref. 48.
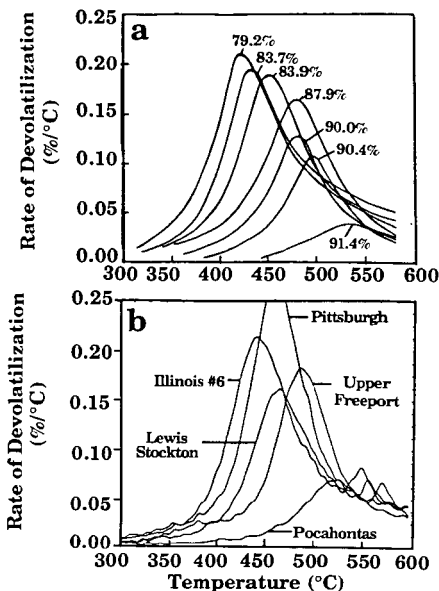

Figure 2. Rate of Devolatilization at a Constant Heating Rate of 3.0°C/min. a) Data of van Krevelen (1), b) Data for Argonne Premium Samples.
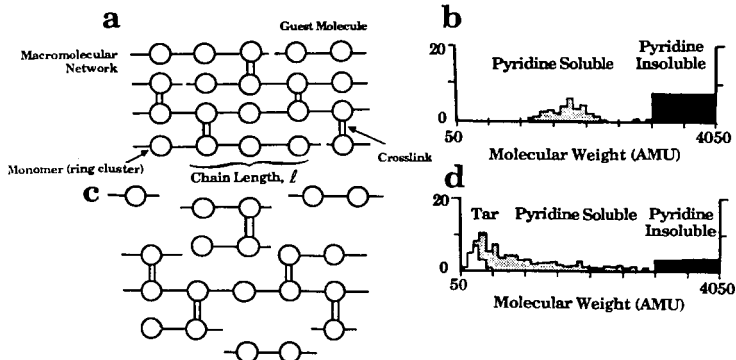

Figure 3. Representation of a Coal Molecular Network in a Monte Carlo Simulation (a and c) and Corresponding Molecular Weight Distribution (b and d). In the Molecule, the Circles Represent Monomers (ring clusters with their peripheral groups). The Molecular Weight Distributions of the Network are Shown as Histograms in b and d. The Histogram is Divided into Tar, Pyridine-Soluble and Pyridine-Insoluble Fractions. The Area Under the Histogram Corresponds to the Weight Percent of the Oligomers.
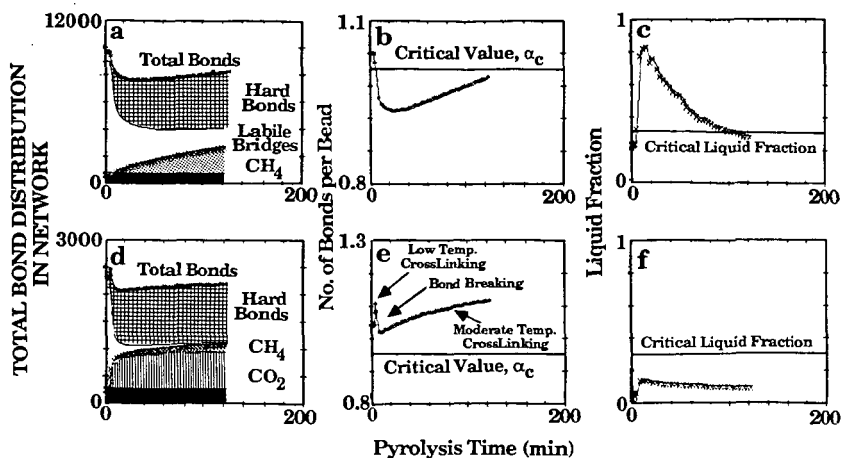
903

Figure 4. Comparison of the Variation in the Unbroken Bond Concentration, Bonds/Cluster, α and Liquid Fraction with Time at Constant Temperature of 440°C for a-c) Upper Freeport Bituminous Coal and d-f) Zap Lignite. ▓ Unbreakable Bridges; ▭ Labile Bridges; ▒ CH₄ Related Crosslinks; ▥ CO₂ Related Crosslinks; ■ Initial Crosslinks.
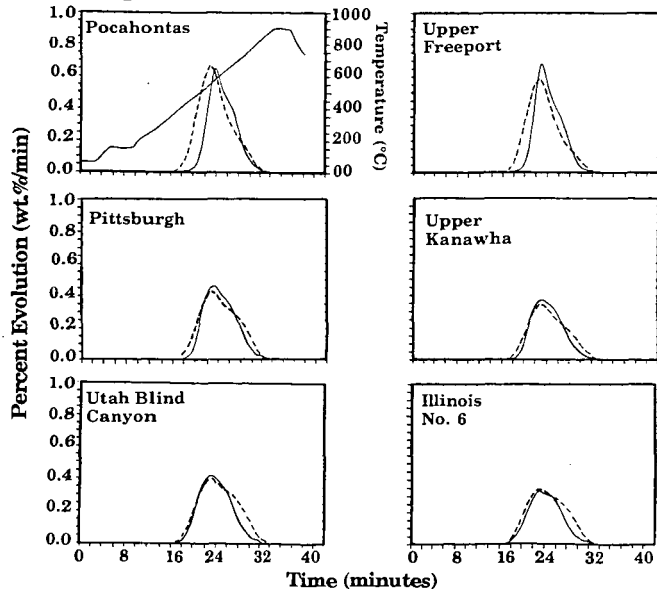

Figure 5. The Evolution of Methane from Argonne Premium Samples in a TG-FTIR at a Constant Heating Rate of 30°C/min (53). Solid Line is Data, Dashed Line is Theory. The Temperature History is shown on the Pocahontas Plot.
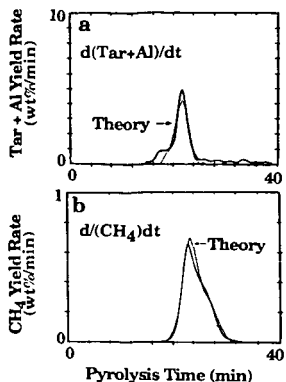
Figure 6. Comparison of Theory with TG-FTIR Experiment on Upper Freeport Coal for the Evolution of a) Tar plus Aliphatic and b) Methane Using the Improved Rates shown in Table 1.
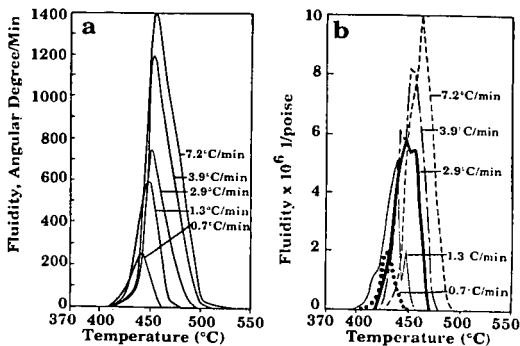
Figure 8. Fluidity at Constant Heating Rate. a) Experiment Data of Van Krevelen (1) for 24% Volatile Coal and b) Theory for Pocahontas Coal Composition (see note in Table 1).
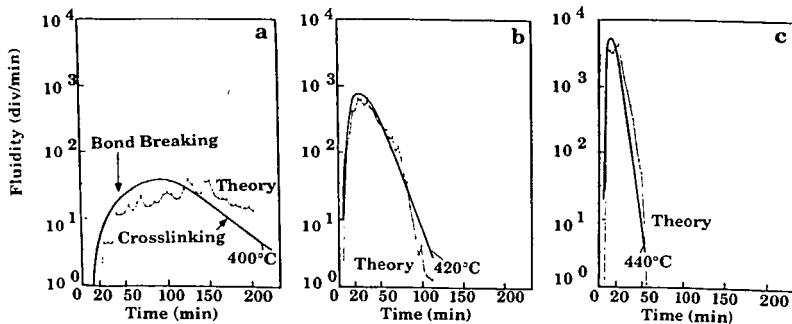

Figure 7. Comparison of Experiment and Theory for Fluidity of a High Rank Coal at Constant Temperatures of a) 400°C, b) 420°C and c) 440°C. The Experiment is for a Coal which has 30% Volatile Matter Content (47) and Theory is for Upper Freeport Coal.
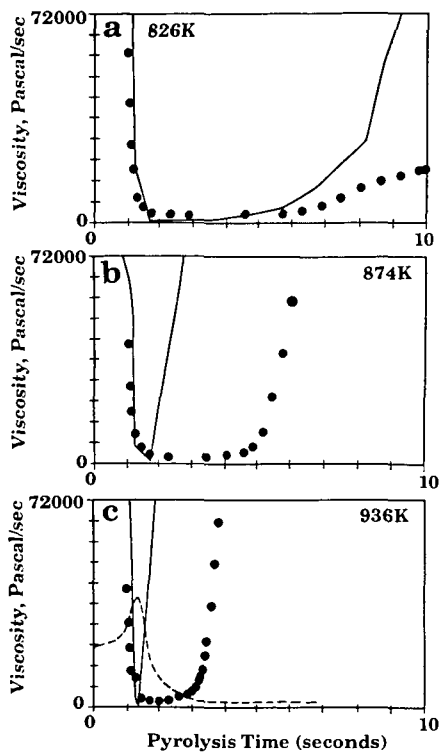
Figure 9. Viscosity at High Temperatures. Symbols are Data of Fong et al. (15).
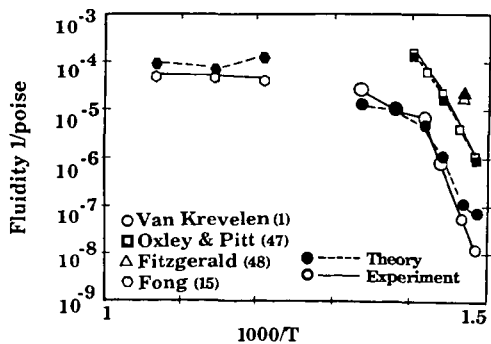

Figure 10. Maximum Fluidity for Four Experiments.

THE PLASTOFROST TECHNIQUE FOR STUDYING
THE CARBONIZATION OF COAL - A RE-EXAMINATION

A.J. Royce, P.J. Readyhough, and P.L. Silveston
Coal Research Laboratory, Department of Chemical Engineering
University of Waterloo
Waterloo, Ontario, N2L 3G1, Canada

Introduction

The Plastofrost technique was developed by Ritter and Juranek[1,2] in West Germany to observe the coal-to-coke transformation (softening, pore development and resolidification), and the interaction of coal macerals at different degrees of carbonization. Changes occurring at different temperatures during the process become visible and if captured on film, produce a time-temperature record of the carbonization stages. Although hailed as a useful technique by researchers the Plastofrost technique enjoyed just a brief period of popularity. Since the 1960's the technique does not appear to have been mentioned in the coal science literature. A recent thesis[3] seems to have rekindled interest in the method.

Our objectives in this paper are to describe the Plastofrost technique and the modifications we have made, illustrate the information obtained, and to examine the range of scientific and technical questions this procedure can be used on.

The principle of the Plastofrost technique is to produce a temperature difference across a coal sample so that the bottom of the sample reaches at least 550°C when the top of the sample has not yet attained 350°C. The maximum temperature ensures that semicoke forms so that the coke texture can be observed, while limiting the top temperature permits dewatering to occur, but not softening. Placing thermocouples in the sample gives the temperature gradient; the temperature at each point in the sample is known and a temperature can be assigned to each visible stage of the coal to coke transformation. Heating of the sample is unidirectional just as in a coke oven. However, in the Plastofrost unit, the sample is heated from the bottom. It differs, therefore, from a coke oven in the direction of gas flow with respect to the temperature front. Some of the gas in a coke oven will move through the hot zone, and undergo further cracking, whereas in the Plastofrost, gas flow is only into the cooler region of the sample. The significance of this difference is not known. Nevertheless, movement of the temperature front through the sample makes the Plastofrost a better model of a coke oven than a dilatometer or a plastometer whose designs emphasize uniform heating.

Equipment

Figure 1 shows a schematic (elevation) of the Plastofrost apparatus as modified for the present study. The two main components are the furnace and the coking attachment. The furnace consists of a nickel-plated copper slab in which four 300 watt cartridge heaters are enclosed. A chromel/alumel thermocouple insulated with ceramic tubing placed 5 mm beneath the top surface of the slab measures the temperature (see Fig. 1). The bead of the TC is at the centre of the slab.

The coking attachment comprises a baseplate; a coking cylinder; and a ram. The coking cylinder has an inside diameter of 41 mm and a height of 75 mm. Wall thickness is 3 mm. The cylinder can be separated vertically into halves and has ten evenly spaced holes 5 mm centers, along each side of the vertical split. Ceramic tubes (2.5 mm o.d.) are placed in these holes, as shown in Figure 1, and chromel/alumel thermocouples are inserted so that the measuring junctions are located along the axis of the cylinder. Halves

of the cylinder are clamped together as shown in the figure.

The cylinder fits into an insert in the baseplate. This plate measures 110 mm x 110 mm and is 6 mm in thickness (Fig. 1). Three 6.3 mm rods, 115 mm in height extend from the base plate to the retainer for the ram. The ram itself is 10 mm thick and has a diameter of 39.75 cm, just slightly less than the inside diameter of the coking cylinder so that it can easily compact and retain the coal within the cylinder. It is fitted with a 76.5 cm long "T-shaped" handle, threaded through the retainer. Thus the ram can be raised or lowered to provide any desired degree of compaction in the coal.

The coking attachment is placed in a snug fitting inset on the top plate of the furnace. This is stepped as shown in the figure to reduce heat flow to the cylinder walls. The furnace provides unidirectional heating to the sample in the cylinder from the bottom upwards.

A microcomputer based control and data acquisition system is required to monitor the 10 thermocouples in the sample and to control the furnace temperature. Details are given by Duever [3] and in a WCPD report [4].

Procedure

Prior to loading, an aluminum foil was placed in the coking cylinder and ceramic tubes, 5 cm in length, were fitted in to the holes located in the coking cylinder. The cylinder was placed on the baseplate before coal was added. A sample of air dried, ground coal, weighing 85 grams, was incrementally packed into the cylinder using the ram to guarantee a constant packing density of 0.9 g/cm^3 for all samples. The attachment was then suitably insulated using fibrefax and insulating tape. Insulation was needed to ensure a uniform radial temperature distribution. The ten chromel/alumel thermocouples were inserted into the ceramic tubes and connected to a junction strip as the last step. In some experiments, only 66.5 g of coal were used to give a density of 0.76 g/cm^3

The samples were heated in air until the temperature in the lowest level of the coal reached 200°C. At that time nitrogen was introduced into the test chamber to prevent oxidation of the sample. The furnace was heated thereafter at the maximum heating rate until its temperature reached 400°C. The temperature in the lowest level of the packed coal sample at this time was usually about 250°C. Above 400°C the furnace heating rate was controlled at 3°C/min. Heating continued until the temperature in the lowest level of the coal reached about 550°C. At this time, the furnace was turned off, the coking apparatus removed from the furnace plate left to cool in an inert atmosphere until the temperature at all levels fell below 200°C. At this point, the foil wrapped sample was impregnated using a polyester resin sometimes thinned with acetone. After hardening the sample was cut into two pieces perpendicular to the ceramic tubes using a diamond-tipped circular saw. Each half was impregnated with polyester resin again, but this time under vacuum.

The final step in sample preparation was grinding and polishing. The former followed the recommendations of the Bituminous Coal Research Inc. [5]. The exposed face of the coked samples were polished to produce scratch-free surfaces suitable for microscopic examination using three polishing stages, each of three minutes duration. After each polishing stage, an ultrasonic cleaner was used to remove all polishing or grinding particles. Using a Zeiss UNIVERSAL Research Microscope, Plastofrost samples were examined by reflected light using parallel polars and a 1/4 λ plate inserted between the specimen surface and the analyzer to characterize the samples in terms of their optical texture. A strip 5 mm wide on either side of the center axis of the cylinder was examined. Juranek et al. [6] measured the temperature profile perpendicular to the center axis and found that within such a strip, deviation from the temperature along the center axis was within 3°C.

The first step in the microscopic evaluation was to determine the relative positions of the ceramic tubes making use of a stage micrometer. These tubes held the thermocouples during the tests so that the exact temperatures at these positions were known. Then samples were examined at 50X magnification in air to observe the softening characteristics of the coal, its resolidification, and the nature of the coke formed. This was accomplished by identifying the following transitions found by Ritter and Juranek [1,2] and Juronek [6] to be common to coking goals.

1) The first appearance of pores in the individual grains.
2) The initial fusion of the grains.
3) The point at which there is a significant increase in the proportion of pores.
4) The completion of fusion where individual grains are no longer distinguishable.
5) The development of anisotropic semicoke.

With the aid of the stage micrometer, positions could be assigned to each of these changes to the nearest tenth of a millimeter and the temperatures for each transition could be estimated from the temperature record.

Completion of fusion and a significant increase in pores are relatively gross characteristics and could easily be identified at 50X magnification. Determinations of initial pore development and grain fusion were more difficult and generally required higher magnifications of 100 and 200X. The anisotropic nature of the semicoke was observed at 200 and 500X magnification. The development of anisotropy in the softened coal moss is an indication of decreasing viscosity. With increasing time and temperature, anisotropic domains grow and may form large regions of uniform orientation. Thus since these domains should not change above the resolidification point, the point at which domains cease to grow and change should be the resolidification temperature.

Further details of procedure are available [3,4]. Several experiments were performed using coal-bitumen slurries. A different procedure had to be developed to prepare samples from slurries. Fluidity of the slurry during heating was a problem. A paper at recent ACS Symposium [7] discusses the procedure developed. An extended discussion appears in a report in the public domain [10].

Plastofrost Observations

As mentioned above, some of the carbonization stages are easily identified. One of these is the completion of fusion. Figure 2 shows the observed completion of fusion in a cretaceous LVB sample. The black and dark grey regions are unfilled and resin filled pores or interparticle voids respectively while the light grey, largely featureless region is the fused vitrinite. Boundaries between bordering vitrinite macerals have disappeared and bridges connect well separated macerals. Devolatilization pores are the irregular sized, semicircular regions in the vitrinite macerals. A distinct inertite maceral, probably semi fusinite, is at the lower left border of the photo. Stress cracks arising during cooling are also visible.

Use of 1/4 λ plate with parallel polarizers permits the texture of the cooled molten phase and the semi coke to be observed. Figure 3 shows the texture of the anisotropy for 3 samples. Magnification of all samples is 200X. The uppermost figure shows elongated, flow domain texture at 458°C that is typical of both carboniferous and cretaceous LVB coals. Texture has been interpreted by Grint et al. [8]. Surprising is that this anisotropy is seen at a temperature 25°C below the temperature of maximum dilatation measured using a Ruhr dilatometer for the coal [4]. The coal must still be fluid at this temperature. Thus, the texture represents either structure in the softened or molten coal or formed as the coal solidifies on cooling in the sample preparation procedure. Appearance of anisotropy prior to the temperature of maximum dilatation, that is, while the coal was still plastic, occurred with both cretaceous and carboniferous MVB coals. It did not occur with the HVB samples.

For these coals, the temperature of maximum dilatation coincided with the temperature of the first appearance of anisotropy so that the latter temperature does signal semicoke formation for this rank of coal.

Coal rank (vitrinoid mean reflectance) affects texture of the semi coke strongly. Figure 3b shows well developed fine mosaic anisotropy surrounding a pore in the lower right of the photomicrograph. The vitrinoid material seems tightly bonded to the unsoftened and unfused semi fusinite that appears in the upper part of the photomicrograph. The coal used for this sample was a cretaceous HVB which had a reduced vitrinite content. The fine to coarse grain texture is typical for the HVB coals. The temperature reached at the point where the photomicrograph was taken was 550°C. The texture seen in Fig. 3b contrasts well with the texture for an LVB sample shown in Figure 3a.

Figure 3c is taken from another, as yet unpublished study of coal carbonization during co-processing of bitumen and coal [7]. The circular black region is a resin filled devolatilization pore surrounded by bitumen semicoke. Fused vitrinite is the bright region with very little texture. The photomicrograph suggests that neither the bitumen or the plastic coal are mutually soluble and the presence of bitumen does not interfere strongly with the fusion of vitrinite macerals.

Plastofrost Applications

The brief discussion of the photomicrograph indicates some of the applications of the Plastofrost technique: development of anisotropic texture as carbonization proceeds; measurement of the softening temperature, the plastic range and, for HVB coals, the resolidification temperature; and pore size, distribution and wall thickness. Beginning with Duever's study [3,9], the Waterloo Coal Research laboratory has applied the Plastofrost to three problems: 1) measuring the effect of metal salts on coal particle fusion during bitumen coal co processing, 2) assessing the accuracy of the dilatometric plastic range, and 3) exploration of the failure of rheological tests to predict the good coking performance of North American cretaceous coals.

In the first of the above three applications [10], two cretaceous and two carboniferous coals were used along with a heavy bitumen (vacuum bottoms). Plastofrost samples were prepared from the coals with 0, 5 and 20 wt% metal salts, the vacuum bottoms, and slurries of 30 wt% coal in the vacuum bottoms with metal salt levels of 0, 5 and 20 wt%. It was found that the salt delayed initial fusion of the coal grains and completion of fusion. The anisotropic texture of the semicoke was diminished by the salt. The presence of vacuum bottoms suppressed coal fusion, probably by physically separating the coal grains. Fusion is also slightly suppressed at 20 wt% additive; 5 wt% seemed to have little effect. Dissolution of vitrine in the bitumen was not observed. The coal and vacuum bottom phases carbonize separately yielding distinct, but well bonded semicokes. Anisotropic texture of the vacuum bottoms coke is strongly diminished by the presence of the finely ground coal. The micrographs suggest that the metal salt impregnated coals expel the salt on softening. This salt collects on the maceral surfaces and may physically interfere with the fusion process.

The second and third applications employed the same Plastofrost data taken with two suites of HVB to LVB coals of the carboniferous and cretaceous eras. The coals were split by gravimetric means into vitrinite enriched and depleted samples. In our study of dilatometry plastic ranges [11], it was found that the plastic range agrees well with the range obtained from the Plastofrost initial softening and first appearance of anisotropy temperatures for coals showing positive total dilatations and HVB coals with high vitrinite content. This is shown in Figure 4. With the exception of several HVB coals, the dilatometer seriously underestimates the plastic range of poorly or non-dilatating coals. The explanation

for this is that dilatometry does not correctly measure the softening temperature of many coals. Only with HVB coals do the estimates of initial softening temperature by the two techniques agree.

As discussed earlier, the Plastofrost estimate of the resolidification temperature (semicoke formation) is incorrect for MVB and LVB coals. Thus, that technique does not give the "real" plastic range. The best estimate seems to come from using the Plastofrost measurement of the initial fusion temperature and the dilatometer reading of the temperature of maximum dilatation.

The third Plastofrost application [4] investigated the observation [12,13] that rheological tests on certain bituminous coals of cretaceous origin indicate that the coals have poor coking quality eventhough commercial use and ASTM Sole Heated Oven tests show that these coals produce good quality coke. The Plastofrost observations indicate cretaceous bituminous coals exhibit all the carbonization stages seen in good coking coals. Temperatures of the carbonization stages do not differ greatly between the carboniferous and cretaceous coals as well. The plastic range of the latter coals is generally smaller for the LVB coals; the difference approaches 55°C. It was concluded that the problem with the rheological tests lies with the assumption that contraction and dilatation depend only on fluidity of the coal. These changes probably reflect the viscosity of the softening coal and the size and distribution of the inert macerals in the coal.

Three years experience with the Plastofrost technique indicate measurements are reproducible, provided the same observer makes the readings. However, sample preparation is slow and measurements have a subjective element because different observers obtain different stage temperatures from the same sample.

Acknowledgements

References

1)   Ritter, H. and Juranek, G., (1960), "Eine Neue Method zur Untersuching und Berschreibung des Erweichungsverhaltens von Kohlen"; Brennstoff Chemie, 41 (6), 170.

2)   Ritter, H., and Juranek, G., (1961), "Ueber das Erweichungsverhalten von Kohlen im Bereich der Oberen Esskohlen bis Unteren Fettkohlen", Brennstoff Chemie, 42, 17.

3)   Duever, P.D., "An Investigation of Coal Rheology with a Plastofrost Apparatus", MASc Thesis, Department of Chem. Eng., University of Waterloo, Canada (1986).

4)   Waterloo Centre for Process Development (1989), "A Plastofrost study of Western Canadian coking coals", Final Report prepared for the Canada Department of Supply and Services and the Canada Department of Energy, Mines and Resources, Ottawa, Canada.

5)   Berry, W.F. and Cole, D.L., (1965), "Preparation and Polishing of Coal and Coke for Petrographic Analysis", Bituminous Coal Research Inc., Pennsylvania.

7)   Royce, A., Readyhough, P.J., Silveston, P.L. and Fouda, S.A., "Effects of Iron Salts on

the Carbonization of Coal-Bitumen Slurries", Symp. on the Chemistry of the Carbonization of Petroleum Feedstocks, Div. of Petroleum Chemistry, ACS Los Angeles Meeting, Sept. 26-30th, 1988.

8)   Grint, A., Swietlik, U. and Marsh, H., "Carbonization and Liquid-crystal (Mesophase) Development-9.   The Co-carbonization of Vitrains with Ashland A200 Petroleum Pitch", Fuel, 58, 642 (1979).

9)   Duever, P.D., Silveston, P.L., and Readyhough, P.J. "Application of a Modified Plastofrost Apparatus to Coal Rheology", CIM Bulletin 80 (901), 60-62 (1987).

10)   Waterloo Center for Process Development "Final Report for Cyclone Engineering Sales Ltd. - Plastofrost Measurements", Univ. of Waterloo, Waterloo, Canada (1988).

11)   Royce, A., Readyhough, P.J., Silveston, P.L., "Plastic Range of Coking Coals" Preprint, Coal Characterization for Conversion Processes Symprosium, Rolduc, Netherlands, May 22-25, 1989.

12)   Berkowitz, N., Fryer, J.F., Ignasiak, B.S., and Szladow, A.J., (1974), "Behaviour Differences Between Carboniferous and Cretaceous Bituminous Coals of Similar Rank:, Fuel, 53 (2), 141.

13)   Leeder, W.R., Gransden, J.R., Price, J.T., and Botham, J.C., (1979), "Prediction of Coke Quality with Special Reference to Canadian Coals", Proc. Ironmaking Conference (AIME) 38, 385.
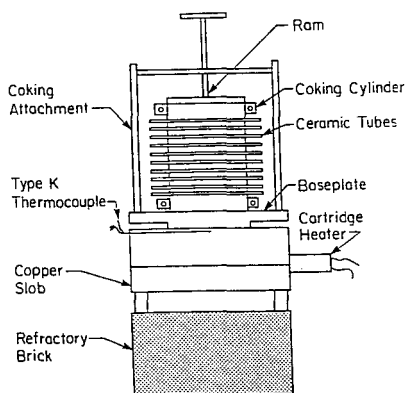
Figure 1   Schematic of the Plastofrost Apparatus

Figure 2   Completion of fusion (413°C) for a vitrinite enriched cretaceous LVB coal
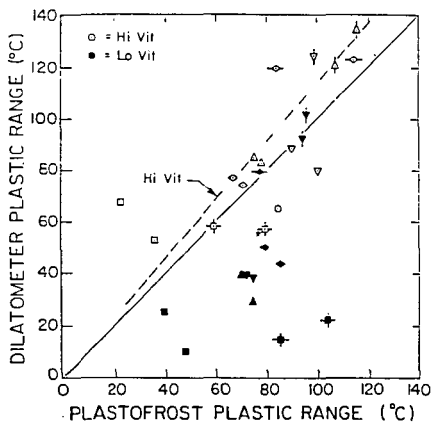

(a)   Flow domain anisotropy in a LVB Semicoke

Figure 4 Cross plot of dilatometric and Plastofrost plastic ranges

INVESTIGATIONS OF THE ROLE OF COAL THERMOPLASTIC PROPERTIES AND COKE STRUCTURE IN GASIFICATION PROCESSES

Man Leung Chan and K. Mark Thomas
British Gas plc
London Research Station
Michael Road
London SW6 2AD
UK

INTRODUCTION

Coal classification schemes have been developed over many years from studies of the physical and chemical properties of coals as a method of dividing coals into various categories according to their behaviour during carbonisation and combustion. Although there is no universally accepted scheme, most coal classification schemes are based on two main types of parameters:- a)volatile matter, and b)caking and swelling properties. The limited scope and empirical nature of the techniques used in classification schemes and their variation with experimental conditions means that classification schemes have only limited applicability when comparing coal behaviour in high pressure gasifiers where the nature of the process is a primary consideration and the experimental conditions are vastly different from those used in the tests.

The thermoplastic properties of coal, as well as characterising the initial agglomeration processes, are important in determining both porous structure and carbon texture of the coke product. Both the coal and coke structures are significant factors in determining gasification behaviour. The coke strength and reactivity during gasification are of considerable significance in fixed bed gasifiers. The agglomerated coke is broken up by the stirrer to facilitate the countercurrent flow of gases and solids(1) and hence, the mechanical strength of the coke may be an important factor. In the case of weak cokes, a wide size range may be produced and increased levels of dust may occur causing a loss of efficiency and throughput. Coke structure is important in determining reactivity towards oxidising gases which is a main gasification step.

The objective of this study is to provide information on the dependence of coal and coke properties under experimental conditions found in fixed bed gasifiers. The direct link between measurements of coal thermoplasticity and coke structure obtained by examining the structure of the carbonised residues from the high pressure thermoplasticity measurements is considered to be an important aspect of the investigation since it eliminates any possible ambiguities in comparing various sets of data. From these considerations and other experiments under simulated gasifier conditions, comparisons with gasifier operational data can be made which should make it possible to develop optimum methods for predicting coal performance in a particular process.

EXPERIMENTAL

The coals used in this study were a strongly caking coal (Coal Oa, NCB Classification Scheme 301a) and a moderately caking coal(Coal Hl, NCB Classification 602)with the characteristics given in table 1.

The high pressure dilatometer used in this study has been described, in detail, elsewhere(2). It operates at fixed pressures up to 10MPa and heating rates up to $60^{\circ}Cmin^{-1}$. In all other respects , the dilatometer geometry and sample preparation were standard(BS1016:Part12) with the exception of the preliminary temperature stabilisation which was not used with heating rates above $3^{\circ}Cmin^{-1}$. The standard deviations of the contraction and dilatation values are estimated to be 5-10% and 10-15% respectively.

The high pressure plastometer used in this investigation has a geometry which is a scaled down version(x50%) of the Brabender Plastometer which has been described previously(3). It operates at fixed pressure up to 10MPa, heating rates up to $40^{\circ}Cmin^{-1}$ and rotational speeds in the range 2-30 revs per minute. A rotational speed of 10 revs per minute and a sample weight of 12.5g (particle size fraction 0.5-1.0mm) were used in all experiments.

The carbonised residues from the high pressure dilatometer and plastometer(HTT 550C, Soak Time 0.1hour) were crushed , mixed with epoxy resin and mounted in the form of discs. These discs were ground and polished. The polished blocks were examined by polarised light microscopy with a X50 objective at an overall magnification of X500 with the polars adjusted close to extinction. The different structural features were classified according to their appearance ,size and shape, in terms of mosaic anisotropy of various grain size, flow type anisotropy and isotropic material. A 300 point count was used for quantitative measurements on each sample. The error in these measurements is estimated to be better than +-5%. The Optical Anisotropy Index (OAI) was calculated according to the equation described previously (4,5) which is given below.

$$OAI=1*I +2*f +3*m +4*c +5*gf +6*f +7*b$$

where f=fine mosaic,m=medium mosaic,c=coarse mosaic,gf=granular flow,f=flow and b=basic anisotropy.

RESULTS AND DISCUSSION

Figure 1 shows a comparison of the plastometry results obtained for Coal Hl with a heating rate of $3^{\circ}Cmin^{-1}$ at pressures of 0.5 and 5MPa. It is clear that a change in pressure has modified the plastometry characteristics. For this particular coal increasing pressure causes a decrease in the coking intensity while the caking intensity remains virtually unchanged. It is interesting to note that the onset of caking is sharper at lower pressure with the initial softening temperature decreasing markedly with increase in pressure. The plastic range also increases correspondingly with increase in pressure. A graph of plastometry parameters against pressure is shown in Figure 2. This clearly illustrates the different behaviour of the caking

and coking intensities with respect to pressure. In contrast, the plastometry parameters of coal Oa show similar trends with the exception of the coking intensity which does not change markedly with changes in pressure. The effect of heating rate on the plastometry characteristics of both coals is quite marked. The plastometry curves show that the caking intensity for both coals is not affected greatly by changes in the heating rate and this is similar to the effect of changes in carbonisation pressure. Figure 3 shows that both the coking and maximum fluidity intensities decrease dramatically with increasing heating rate. The apparent plastic range also increases with heating rate.

To understand the changes in plastometry characteristics, the swelling during carbonisation needs to be considered. Previous work has shown(2,4-8) that the swelling characteristics of coals are markedly dependent on heating rate and pressure, and cannot be predicted accurately from their swelling under standard conditions(atmospheric pressure and low heating rate). The three types of dilatation behaviour with respect to pressure which have been observed, depend to some extent on coal rank and are as follows:

    a) an increase in dilatation with pressure;
    b) an increase to a maximum at 1-1.5MPa followed by a decrease;and
    c) a decrease in dilatation with pressure.

In contrast, the dilatation of coals as measured by the method used in this study, increases with increasing heating rate. A limiting value of the dilatation was observed at a heating rate of $20^{\circ}Cmin^{-1}$ in a previous study(4). An increase in pressure will have two main effects:a) a reduction in the volume of gas trapped in the fluid phase which would tend to decrease the swelling; and b) an increase in the secondary reactions by decreasing the volatility of tar and increasing the residence time in the fluid phase which would tend to increase dilatation. The changes in dilatation behaviour can be rationalised by considering the balance between the release of gaseous and liquid volatiles. The variation of the dilatation of coal Oa with heating rate at 2MPa pressure is shown in Figure 4. The dilatation of coal Oa increases with heating rate but decreases with increase in pressure(0.5-5MPa). A graph of dilatation against plastometry torque parameters for a range of heating rates(3-20°Cmin^{-1}) with a carbonisation pressure of 2MPa is shown in Figure 5. This graph clearly shows that there is a correlation between some of the plastometry and dilatometry parameters. It is noticeable that the caking intensity is not as sensitive to changes in dilatation as the coking and maximum fluidity intensities which change significantly.

Investigations of the optical anisotropic content of cokes derived from a wide range of coals have shown that it is a useful parameter for characterising their structure. Previous work has shown(4,5,9) that changes in carbonisation pressure and heating rate can have a considerable effect on the optical anisotropic

content of cokes.In particular, the anisotropic content of cokes usually increases substantially with pressure at heating rates of $40^{\circ}Cmin^{-1}$ to a limiting value above approximately 3MPa. The corresponding increase in anisotropic content appears to be much smaller at low heating rates. However, there is only a limited amount of information available in the literature on this aspect. In general, the change in OAI development in relation to pressure varies with rank in a fairly systematic manner but there is no direct correlation between individual rank and anisotropy parameters. The results suggested that the OAI changes are related to the influence of pressure on the retention of plastic material and modification of the plastic range. The variation of optical anisotropy index(OAI) for cokes derived from coal Oa at a carbonisation pressure of 2MPa with heating rate is shown in Figure 6. It is apparent that the OAI increases with increasing heating rate. For this particular coal, the changes in OAI also correlate with some of the plastometry parameters ,in particular,the coking intensity, the intensity at the point of maximum fluidity and the plastic range. Further work is needed on a wide range of coals to establish definitive correlations between plastometry parameters, swelling characteristics and coke porosity and structure.

CONCLUSIONS

The relationship between coal thermoplastic properties and coke structure is very complex. The results of this investigation have shown that these properties are strongly dependent on the experimental conditions and, in particular:

a)increased swelling is accompanied by a decreased plastometry coking intensity.

b)The plastometry caking intensity is considerably less sensitive to change in experimental conditions than the other plastometry parameters.

c) The optical anisotropy index is increased by heating rate and this is accompanied by changes in plastic range, plastometry coking intensity and a decrease in the apparent viscosity at the point of maximum fluidity.

These changes can be rationalised by considering the release of gaseous and liquid volatiles during the carbonisation of the coal. The lack of sensitivity of the caking intensity to heating rate and pressure is consistent with its origin being partly softening prior to the major decomposition. Further work is needed to relate coal thermoplasticity measurements to other coke structural data ,in particular, texture and porosity measurements.

REFERENCES

1. Thomas, K. M. in 'Carbon and Coal Gasification-Science and Technology'(Eds. J. L. Figueredo and J. A.Moulijn),Nato ASI E105, Martinus Nijhoff,Dordrecht,1986,p439.

2. Green, P.D. and Thomas,K.M. Fuel 1985,64,1423.

3. Mulligan, M. J. and Thomas, K. M. Fuel 1987,66,1289.

4. Green,P.D., Patrick,J.W., Thomas,K.M. and Walker,A. Fuel 1985,64,1431.

5. Green,P.D.,Patrick,J.W.,Thomas,K.M. and Walker,A. Proceedings of International Gas Research Conference 1986,p1053.

6. Kahn, M.R. and Jenkins, R.G. Fuel 1984,63,109.

7. Beyer,H.D. 'Caking and Coking Power of Bituminous Coals Under High Pressure'. Report BMFT-FB-T 82-055.

8. Kahn, M.R. and Jenkins, R.G. Fuel 1986,65,725.

9. Green,P.D.,Patrick,J.W.,Thomas,K.M. and Walker,A. Fuel 1989,68,149.

Table 1
Characterisation Data for the Coals used in this Study

|	Coal Oa	Coal Hl
Rank	301a	602
Proximate Analysis(wt%dry basis)		
Volatile Matter	18.9	38.7
Ash	9.2	3.8
Ultimate Analysis(wt%dry basis)		
Carbon	82.6	79.6
Hydrogen	4.3	5.3
Chlorine	0.05	-
Sulphur	0.86	1.65
Caking and Swelling Properties		
Swelling Number	6	3
Dilatometry		
Dilatation(%)	41	36
Contraction(%)	23	30
Plastic Range(^{o}C)	87	73
Gieseler Plastometry		
Max.Fluidity(ddpm)	590	535
T_3-T_1(^{o}C)	91	69
Petrographic Analysis		
Reflectance(%)	1.46	0.71
Maceral Analysis(vol.%)		
Vitrinite	65	78
Exinite	-	9
Inertinite	35	13
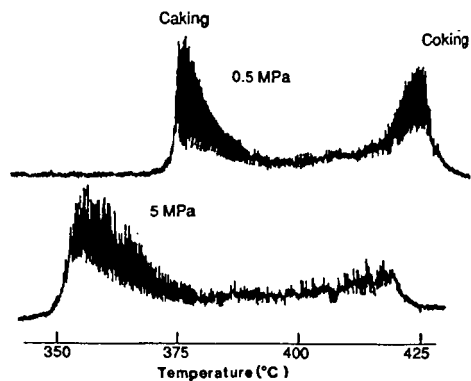
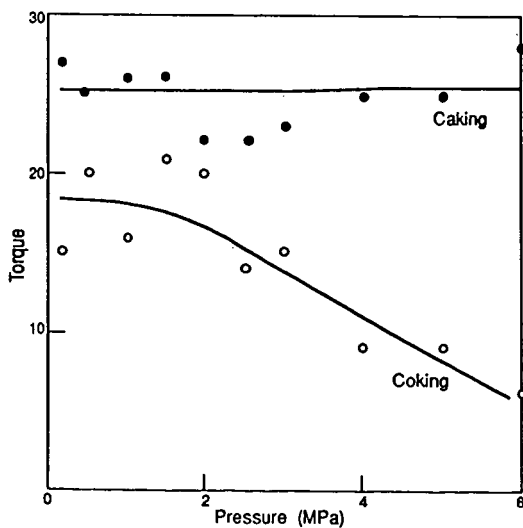**Fig. 1. A comparison of the plastometry curves for coal HI at 0·5 and 5MPa (heating rate 3°C min⁻¹)**

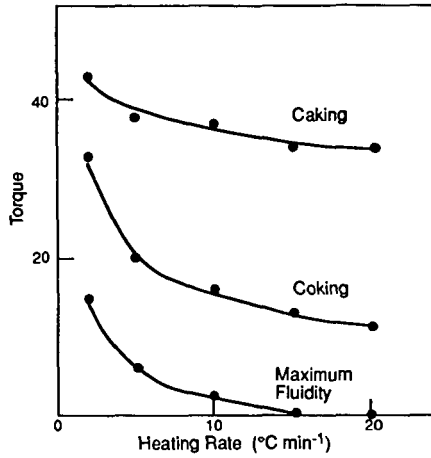**Fig.2. The variation of plastometry torque parameters with pressure for Coal H1 (Heating Rate 3°C min⁻¹)**

Fig.3. The variation of plastometry torque parameters
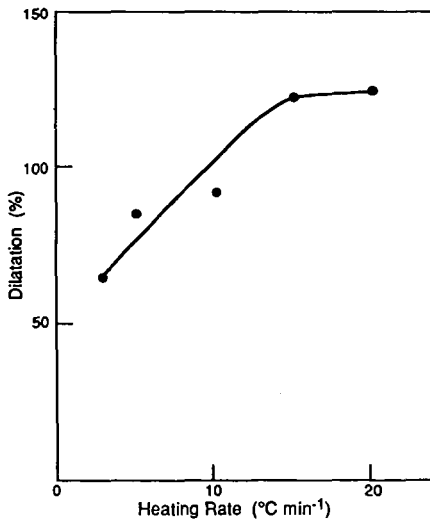with heating rate for coal H1 (Pressure 2 MPa)

Fig.4. The effect of heating rate on the dilatation
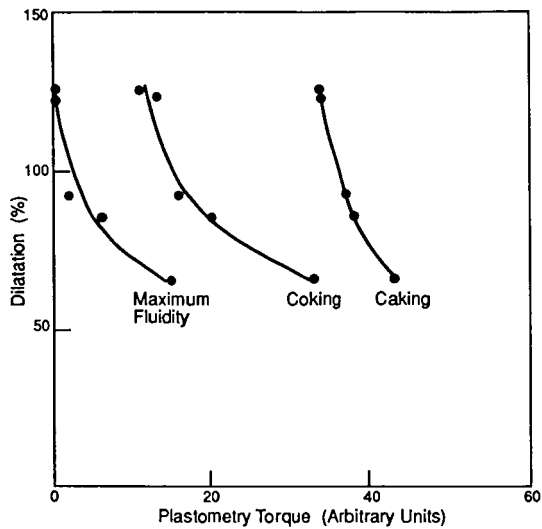of coal Oa (Gauge pressure - 2 MPa)

Fig.5. The variation of dilatation with plastometry torque
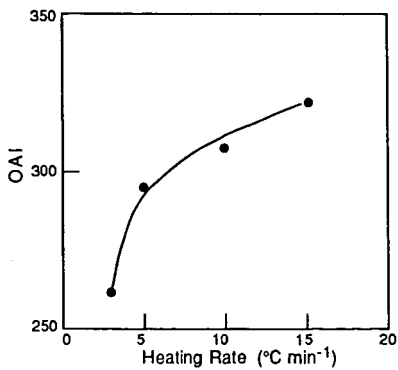parameters at 2 MPa pressure for coal Oa

Fig.6. The variation of optical anisotropy index (OAI)
with heating rate for coal Oa (Pressure 2 MPa)

922

THE EFFECTS OF OXIDATION AND WEATHERING ON COAL COMBUSTION

S.L. Bend, I.A.S. Edwards and H. Marsh.
Northern Carbon Research Laboratories,
Dept. of Chemistry
University of Newcastle upon Tyne. NE1 7RU
United Kingdom

INTRODUCTION

General Review of Coal Oxidation

The low temperature oxidation of coal dramatically influences and alters inherent properties. The deleterious effect that oxidation has upon the coking and caking properties of coals, through the loss of plasticity and fluidity, is well documented [1,2,3]. The oxidative mechanism and processes by which coal properties are affected are discussed at length in the literature. Puttnam et al [4], examining a suite of naturally weathered coals, discuss the possible transformation of aromatic compounds within the extractable organic material into molecules containing polar substituents. Larsen et al [2] suggest that the plasticity and fluidity of vitrinite rich coals can be lost by the oxidation of reactive benzylic positions and their replacement by carbonyl and carboxyl functional groups, with the concomitant loss of donatable hydrogen from the coal structure. In addition, an increase in cross-link density, due to the introduction of oxygen-bearing functional groups into the macromolecular structure of the coal, may prevent depolymerisation and plasticity during char formation.

Coal Oxidation Related to Combustion

Nandi et al [5], in their investigation into the role of inert coal macerals in pulverised fuel combustion, determined that the combustion efficiencies of coal were inversely related to the (organically) inert content of the coal feedstock during pilot-scale combustion experiments. Included in their category of organically inert material were what they considered to be oxidised vitrinite. Axelson et al [6], investigating the effects of oxidation upon in-situ outcroppings and stockpiled coal, discuss the problems encountered when attempting to characterise oxidised coal using conventional techniques, noting the additional complicating factors petrographic composition has upon techniques such as Free Swelling Index. They concur with earlier studies [2] that postulated different mechanisms for oxidation to occur above and below 80°C.

However, few studies discuss the effect that the oxidation of pulverised-coal feedstock has upon pyrolysis and combustion using Entrained Flow Reactor (EFR) apparatus. With increasing world coal trade that often requires the temporary stockpiling of coal, either prior to, or subsequent to, shipment to various points of usage, the effects of oxidation upon coal feedstock requires some attention. There are no grounds for assuming that the specifications quoted by the coal vendor or that the published characteristics of commercial steam coal are fixed and remain constant in time.

OBJECTIVES

The overall objective of this study is to investigate the effect of oxidation upon the pyrolysis and combustion of pulverised coal feedstock using laboratory based equipment. More specifically the study aims to:
1. Investigate the effect of artificial oxidation upon the intermediate char morphology of pulverised fuel.
2. Investigate the effect of natural weathering upon the intermediate char morphology of pulverised fuel.
3. Assess the suitability of existing coal characterisation techniques when seeking to determine the effects of oxidation upon coal feedstock.
4. Suggest new ways of characterising oxidised coal feedstock.

EXPERIMENTAL

Materials Used
The three freshly mined Carboniferous bituminous coals used in this study were supplied by British Coal and originate from coal mines within the Northumbrian coalfield (UK). Coal 88/024 and 88/026 are both British Coal (1964) class 500's, whereas coal 88/025 is a class 700 (steam raising coal). Their characteristics are given in Table 1.

Table 1. Some of the characteristics of the fresh coals used in this study

Coal	Rank (ASTM)	Ro max (%)	Maceral analyses (%)				Proximate analyses (wt %dry)	
			Vitrinite	Liptinite	Inertinite	Mineral Matter	V.M.	Ash.
88/025	Hvb B	0.73	61.2	14.4	23.8	0.6	39.0	4.8
88/026	Hvb A/B	0.79	76.4	12.2	11.6	0.0	35.0	10.02
88/024	Hvb A	0.93	72.2	12.4	14.8	0.6	37.0	5.1

Sample Preparation
The three freshly mined samples of coal were received in lump form (>10 cm^{-1}) within hours of being mined. They were crushed to (>2.5mm) in a mechanical jaw crusher and each coal subdivided into twelve individual samples, representing two sets of six per coal. One set of five samples from each of the three coals was placed in a covered (lined) container and placed in the open air. The second set of five samples from each of the three coals was placed in a large heated receptacle and oxidised at 100°C (± 5) in static air. The sixth sample from each was analysed immediately and used as the datum sample. Samples of weathered and oxidised coal were removed periodically for analysis, thereby providing both artificially oxidised and 'weathered' samples.

Analytical Techniques
A Stanton Redcroft STA 780 TGA was used for all **proximate analyses** [7]. Calorific value determinations were obtained using a Gallenkamp Adiabatic bomb calorimeter. A Carlo Erba 1160 Carbon, Hydrogen and Nitrogen elemental analyser was used for the **elemental analysis**, oxygen was determined by difference. The **Infra-red spectra** of the coals were produced using a Nicolet 20SXB Fourier-transform Infra-red spectrometer with the KBr pellet technique. Each spectra was generated using a total of 30 scans per sample.

Petrographic Analyses
All petrographic analyses of the coals were performed on a Leitz MPV3 microscope photometer. **Vitrinite reflectance** was determined using non-polarised light (%R$_{oil}$ random) on a crushed grain mounted block and based upon 100 measurements. The **maceral analyses** represent a total of 500 individual counts on grain mounted blocks, using a Swift point-counting device and interpoint and interline distances of 50μm. **Quantitative fluorescence microscopy** on grain mounts of un-crushed coal was achieved using an HBO 100 mercury lamp, an EMI S20 photomultiplier tube (PMT), Ploempak, a Zeiss 'Plan Neofluar' x40 0.9n.a. triple-immersion objective (using water), a masked uranyl glass standard and the filter block combinations Tu and I2 (BP 450-490, RKP 510, LP 515). Fluorescence intensity measurements were conducted at 650 nm using a 20 μm measuring spot and the I2 filter block combination. A black cavity cell was used to compensate for parasitic reflections and for zeroing the photometer and calibration of the photometer was achieved using an uranyl glass in which the V.D.U. was set to read 100% [8]. Fluorescence intensity measurements scanned across coal particle surfaces was accomplished using an EMI S20 PMT supplemented by a Hamamatsu R446 PMT, which was attached via the camera tube on the microscope trinoccular head. The EMI S20 PMT was used for the measurements conducted at 650 nm and the HTV R446 PMT was used for measurements conducted at 546nm, thereby enabling simultaneous measurements at both wavelengths on the same field-of-view. The interpoint distance of 20 μm was achieved using a stepping stage set, with a procedure that involved examining the field-of-view using the Tu filter block, focussing, measuring the reflectance at 546 nm (%R$_{water}$, n = 1.3 @ 23°C) using the stabilised tungsten lamp, switching over to the I2 filter block and opening the synchro-compur shutter, positioned in front of the mercury lamp, for the duration of the measurement (2 sec) at

924

I_{650}. A new measuring area was then selected using the stepping stage and the process repeated.

Chars were produced from the coals (38 to 75 μm size fraction) in an Entrained Flow Reactor [EFR] (Figure 1.) in N_2 at $1273 \pm 5K$, consisting of a reaction tube of 1.66m in length using a gas flow rate of 38 1 min^{-1}, to give laminar flow conditions and a residence time of 1 second. **Char morphology** was analysed in terms of type (from Cenospheres, through Network, to Solid types), depending upon the extent of vesiculation and the porosity of the char, using a Swift point-counter and the Leitz MPV3. The anisotropy of the char types was also recorded using a light microscope (x800 overall magnification) and a Swift point-counter. The internal porosity of each char was derived by Image Analysis using transmitted light on thin sections (5μm thick) of epoxy mounted char.
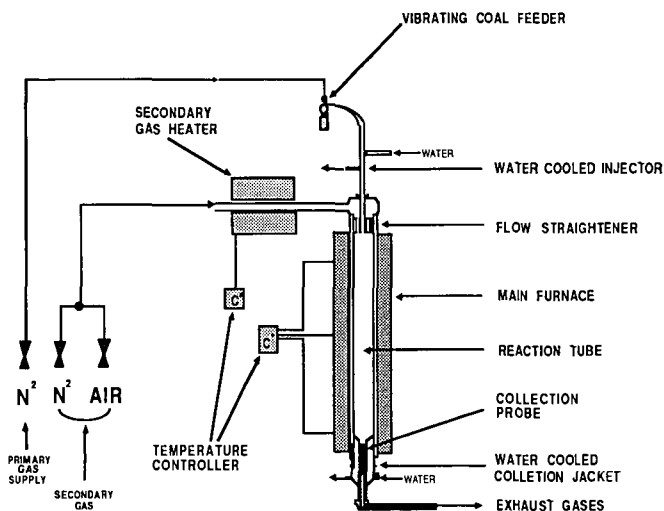

Figure 1. A schematic diagram of the EFR apparatus used in this study.

RESULTS and DISCUSSION

Proximate Analyses

The proximate analyses of the oxidised coals show an initial rapid loss in their volatile matter content, as demonstrated in Figures 2 and 3, with a gradual decrease in the rate of loss as the duration of oxidation increased. For all coals ,the rate of volatile matter loss is greater in the artificially oxidised series of coals than for the naturally oxidised coals over a similar period of time, although, in the case of the 88/024 weathered coal series the volatile matter content loss is less than coal series 88/025 and 88/026 over the same period of time reflecting the influence of rank. Despite initial differences in volatile matter content, reflecting the differences in petrographic composition (Table 1.), weathered coals from the 88/025 and 88/026 series attain similar values after 19 weeks and decrease by the same amount over the two successive sampling points.
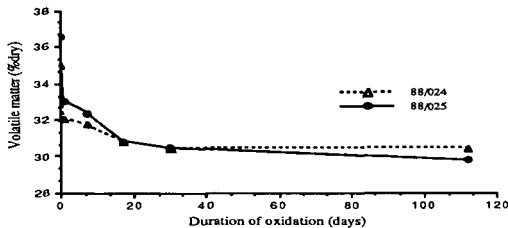
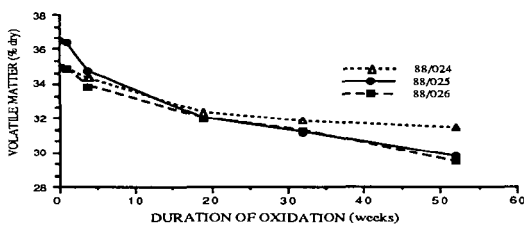Figure 2. Volatile matter yield and artificial oxidation (air/100°C)

Figure 3. Volatile matter yields and natural oxidation (weathering)

7

These observed trends are augmented by a similar decrease in elemental hydrogen and elemental carbon in preference to oxygen and by a decrease in the calorific content of the coal, as noted previously in a study discussed by Axelson et al [6].

Infra-red Analysis and   Functional Groups

Infra-red investigations suggest that the main processes taking place involve the progressive removal of aliphatic hydrocarbons and the inclusion of oxygen bearing functionalities within the molecular structure of the coal. The removal of aliphatic hydrocarbons, such as CH_2 and CH_3, is indicated by a decrease in the absorption bands at 2920, 2850 and 1435 cm^{-1} and is accompanied by the development of absorption bands at 1620-1700 cm^{-1} (ketones), 1690-1718 cm^{-1} (carbonyls in acids), 1765 cm^{-1} (esters) and 1843 cm^{-1} (anhydrides) [9,10]. The development of ring-bound, conjugated, oxygen bearing functionalities is supported in this study by quantitative fluorescence microscopy.

Petrographic analysis of the coals

The vitrinite reflectance values (Figure 4.) increase to approximately 20 to 25% in the artificially oxidised coal series above those values derived from the fresh coals after a period of three months although the reflectance values determined upon the weathered coals decrease over the same period of time. This concurs with the work reported by Puttnam et al [4]. The reflectance values determined in this study on oxidised and weathered coals represent measurements on crushed particles of varying size (>212μm) embedded within the grain mounted block. The findings within this study relating to the trends outlined for the artificially

926

oxidised coals concur with those of Prado [11] i.e. that the reflectance varies across the surface of a particle. Both Prado [11] and Cronauer et al [12] comment on the absence of visible oxidation rims on low temperature
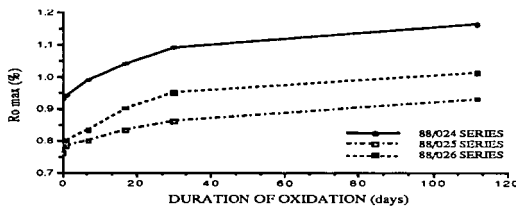

Figure 4. Vitrinite reflectance variation due to artificial oxidation (air/100°C)

artificially oxidised coals when using plain polarised light. Cronauer et al. [12], artificially oxidising coals under similar conditions to those reported here, considered the kinetics of low temperature oxidation to be diffusion controlled but failed to detect the presence of oxidation rims. They were, therefore, unable to verify their reaction concept. However, in this study, when observing the present series of low temperature artificially oxidised vitrinite coal particles in fluorescent mode, rims of low fluorescence activity (quenched fluorescence) as a direct consequence of oxidation for periods of up to one week, are clearly visible. Therefore, the development of conjugated oxygen bearing groups is supported by the observed quenching of fluorescence in oxidised coals. Ring-bound ketones, for example, have $\pi \to \pi^*$ and $n \to \pi^*$ absorbancies at 245 nm and 435 nm. The bond between the ketone and the aromatic group is associated with the $\pi \to \pi^*$ transition, whereas ketones give rise to the $n \to \pi^*$ transition. The electronic transitions of oxygen bearing groups increase in both wavelength and intensity with an increasing degree of conjugation. Fluorescence intensity measurements conducted at 650 nm across the polished surface of vitrinite particles (Figure 5) would appear to verify the oxidation kinetics postulated by Cronauer et al [12], that the reaction appears to be predominantly diffusional at 100°C and under similar conditions. The rims of quenched fluorescence widen as the period of
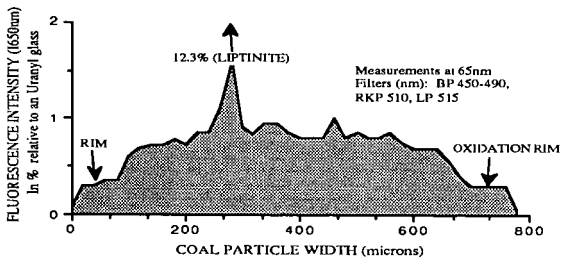
Figure 5. The measured fluorescence intensity across the surface of an oxidised particle of coal (100°C/ air, one day).

artificial low temperature oxidation increases, until eventually no measurable, or visible, fluorescence remains. However, in the case of the weathered coals no well defined oxidation rim exists in the vitrinite particles. Instead the fluorescence intensity diminishes gradually across the particle surface which would suggest that, under the conditions of weathering used in this study, the reactions are probably due to a combination of chemical control and diffusion.

927

Char morphology

The effects of low-temperature artificial oxidation upon the morphology of chars produced in the EFR are well illustrated by the coal series 88/024 (Figure 6) and the oxidised coal 88/025 series (Figure 7). Both unoxidised coals 88/024 and 88/025 are vitrinite rich (see Table 1.) and are of sufficient rank to produce a predominance of cenospheric char forms [Plate 1.].

Proportion of
anisotropic char   92.4%   34.2%   2.2%   0%   0%   0%
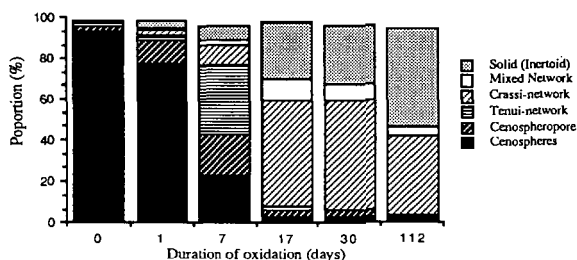

Figure 6.   EFR chars and the artificial oxidation of coal 88/024

Proportion of
anisotropic char   46.2%   27.8%   1.4%   0.8%   0%   0%
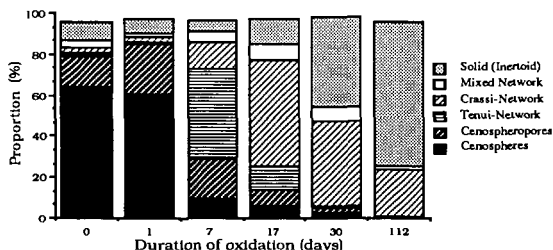
Figure 7.   EFR chars and the artificial oxidation of coal 88/025

The proportion of cenospheres produced during pyrolysis from the unoxidised coals and the percentage of char exhibiting visible anisotropy follows the rank dependence postulated previously [13]. However, the effects of artificial oxidation are most severe on the higher rank series 88/024. The decrease in the proportion of anisotropic char, from an original value of 92.4% down to 34.2% after oxidation at $100^{\circ}C$ for one day ,is notable. This is followed by a virtual elimination of all visible anisotropy in the chars after oxidation for one week. Furthermore, the systematic replacement of cenospheres by isotropic chars of a less-vesiculated nature, i.e. the tenui-network chars [Plate 2.], until the predominant char type is a dense and solid *inertoid* char type of low porosity [Plate 3.] as oxidation time increases (Figures 6 and 7) is a clear indication of the loss of thermoplastic properties during pyrolysis.

928

Deshpande et al [14] discuss the nature of molecular cross-linking and volatile evolution during the pyrolysis of coal in relation to the rank of the feedstock and the decomposition of carboxyl groups during pyrolysis. During the slow pyrolysis of a lignite ($0.5^{\circ}C\ s^{-1}$), cross-linking starts to develop prior to the evolution of tar. At higher heating rates ($2.0 \times 10^4\ ^{\circ}Cs^1$), cross-linking occurs simultaneously with tar evolution. Similarly, the thermoplasticity of a bituminous coal has been attributed to both the presence of cross-links in the macromolecular framework of the coal (vitrinite) and the behaviour of the "mobile phase" during pyrolysis [15]. Upon heating, the macromolecule decomposes and the coal exhibits visco-elastic properties allowing the aromatic units to slide over one another. The volatile matter, which is generated within the macromolecular framework, expands causing the viscous mass (proto-char) to expand during the simultaneous expulsion of gaseous material. The result is the production of a char, the morphology of which is largely dependent, according to the model of Spiro, upon the behaviour of the mobile phase during char formation.

Char formation cannot be readily explained by visco-properties alone. The formation of radicals is also significant during pyrolysis. The formation of radicals, which are highly reactive. Under the operating conditions of the E.F.R., and their probable stabilisation and transformation into volatile species, is possibly achieved primarily by hydrogen addition. The formation of the char particle is followed by the polymerisation and condensation reactions that occur during the recombination of non-volatile radical components. Therefore, the depletion of donatable hydrogen species through the oxidative replacement of reactive benzylic CH_3 or CH_2 groups possibly leads to a greater number of non-stable oxygen bearing radical components during pyrolysis. Solomon and Haublen [16] formulated a 'functional group model', in which coal pyrolysis is regarded as a depolymerisation process that operates parallel to the decomposition of functional groups, in which the pyrolysis products compete for hydogen-capping moieties for stabilisation. According to this model, the type and number of functional groups therefore control the kinetics and mechanisms that operate during pyrolysis.

There is some confusion in the literature [17] regarding the effects of oxidation on vitrinite reflectance. Such confusion exists because the oxidation of coal is dependent upon particle size and the temperature under which the gas-solid reaction takes place. In oxidative techniques that employ high temperatures, there is a 'reaction front', visible as a rim (heterogeneous gas-solid reaction), under low temperature conditions, such as natural weathering, there is no discernible reaction front and the oxygen appears to react progressively throughout the particle (homogeneous gas-solid reaction). Measurements conducted, wittingly or otherwise, on the central area of the particle *beyond the gas-solid reaction front* will lead to variations in reflectivity not necessarily due to the chemical process of oxidation.

Bulk analytical techniques, such as proximate analysis, do not adequately predict the behaviour of oxidised *pulverised fuel during pyrolysis or combustion. The techniques discussed above indicate values associated with* coals of higher rank, although the behaviour of the oxidised coal during pyrolysis is more akin to low rank coals or coals containing a high proportion of the maceral inertinite. Therefore, careful monitoring of properties is necessary when stockpiling coal and the utilisation of petrographic techniques, such as fluorescence microscopy and the saffran-o staining technique [6] will help to discriminate between oxidised and unoxidised coals.

CONCLUSIONS

The progressive oxidation of coal feedstock severely alters the nature and morphology of the char produced during EFR pyrolysis. More specifically:

1. Artificial oxidation of the coal leads to a reduction in the porosity of the char, through a decrease in the extent of devolatilisation and a probable increase in the extent of cross-linking. Furthermore, there is a decrease in the anisotropy of the char as a result of oxidation.
2. The effect of weathering is similar to those witnessed by artificially oxidised coals, although the time required for comparable changes is much greater.
3. Existing coal characterisation techniques do not adequately assess the effect or extent of oxidation and some techniques, such as vitrinite reflectance show variations not necessarily due to oxidation, but more to the *experimental conditions (temperature) employed.*
4. Petrographic techniques, such as fluoremetry, are sensitive to the type and extent of oxidation and therefore represent a useful means of characterising oxidised coal feedstock.

929

References:

[1] Neavel, R.C., in 'Coal Science', (Eds. M.L. Gorbaty, J.W. Larsen, and I. Wender) 1982 2
     Academic Press, New York. 1
[2] Larsen, J.W., Lee, D., Schmidt,T., and Grint, A., 1986 Fuel 65 595
[3] Pis,J.J., Cagigas,A., Simon,P., and Lorenzana, J.J., 1988 Fuel Proc. Technol. 20 307
[4] Puttmann, W., Steffens, K. and Kalkreuth, W. 1987 Int. Conf. on Coal Science (Moulijn J.A.,
     Nater,K.A., Chermin,H.A.G. Eds.) Elsevier 411
[5] Nandi,B.N., Brown,T.D. and Lee,G.K., 1977 Fuel 56 125
[6] Axelson, D.E., Mikula,R.J. and Munoz,V.A. 1987 Int. Conf. on Coal Science (Moulijn J.A.,
     Nater,K.A., Chermin,H.A.G. Eds.) Elsevier 419
[7] Ottaway, M. 1982 Fuel 61 713
[8] Diesel,C.F.K and McHugh,E.A., 1986 Gluckauf-Forschungshefte 47 60
[9] Painter,P.C., Snyder,R.W.,Starsinic,M. and Coleman,M.M. 1981 Applied. Spectroscopy 35 375
[10] Calemma,V.,Rausa,R.,Margarit,C.N. and Giradi,B. 1988 Fuel 67 764
[11] Prado,J.G. 1977 J. of Microscopy 109 85
[12] Cronauer,D.C., Ruberto, R.G., Jenkins, R.G., Davis,A., Painter,P.C., Hoover,D.S.,
     Starsinic, M.E. and Schlyer, D. 1983 Fuel 62 1125
[13] Bend,S.L., Edwards,I.A.S. and Marsh, H., 1988 'Carbon '88' (McEnaney,B. and Mays,T.J. Eds,)
     IOP Bristol 594
[14] Deshpande,C.V., Solomon,P.R. and Serio, M.A. 1988 ACS Div. of Fuel Chem. 33 No 2 310
[15] Spiro ,C.L. in 'Space filling models for coal : A Molecular Description of Coal Plasticity'
     1981 Internal Report. General Electric. Schenectady, New York
[16] Solomon. P.R. and Hamblen,D.G. in 'Chemistry of Coal Conversion' (Schlosberg R.H.
     Ed) 1985 Plenum Press. New York 121
[17] Stach,E., Mackowsky, M-Th., Teichmuller,M., Taylor,G.H., Chandra,D. and Teichmuller,R. 1982
     Textbook of Coal Petrology. 2nd Rev. E.d Gebruder Borntraeger Berlin 535
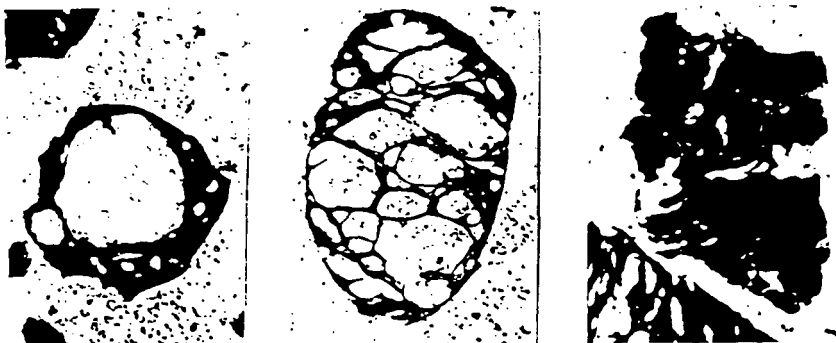
Plate 1.   Plate 2.   20μm   Plate 3.

Transmitted light photomicrographs taken through thin sections of epoxy mounted char, showing the
cross-sectional morphology and internal porosity due to variations in vessiculation and devolatilisation. Plate 1.
shows a Crassicenosphere (thick-walled cenosphere): 68% porosity. Plate 2. shows a Tennuinetwork char: 65%
porosity. Plate 3. shows a Crassinetwork char (bottom left):43% porosity; and an Inertoid, in which no
vessiculation pores are visible although shrinkage cracks are visible: 15% porosity

EFFECT OF OXIDATIVE WEATHERING ON ALIPHATIC STRUCTURE OF COAL

J. T. Joseph and O. P. Mahajan

Amoco Oil Research Department
Amoco Research Center
· P. O. Box 400
Naperville, Il 60566

ABSTRACT

Oxidative weathering of coal affects its structure and properties, and as a result, its utilization. For example, weathering adversely affects liquefaction yield, cokability, calorific value, and beneficiation. However, little is known about the chemistry of coal weathering. This paper discusses the effect of weathering on the aliphatic crosslinks that connect the aromatic-hydroaromatic units in coal. These crosslinks play a significant role in coal liquefaction and weathering alters them.

We have demonstrated, by acid-catalyzed transalkylation reactions and by GC-MS analysis of the products, that oxidative weathering reduces concentrations of several types of straight chain and branched chain aliphatic crosslinks. Infrared spectroscopic analysis shows that these crosslinks are converted to carbonyl and carboxyl groups. Plausible mechanisms for these transformations have been suggested.

INTRODUCTION

It is well known that oxidative weathering of coal induces irreversible structural changes that are detrimental to its utilization. For example, weathering decreases solvent extraction yields[1], coal liquefaction yield[2-5] and hydrocarbon yield during pyrolysis[6]. It also reduces fluidity [5,7,8] and calorific value[9], and causes poor coking behavior[10,11]. Irreversible changes in surface properties, that in turn affect coal beneficiation, also occur during weathering[12,13]. Effects of oxidative weathering on coal properties have been recently reviewed by Berkowitz[14] and by Gray and Lowenhaupt[15].

Relatively little is known about the chemistry of coal weathering. It is known that the oxygen content of coal increases during weathering[16]. The changes in structural features due to weathering have mostly been monitored by infrared spectroscopy.   Painter et al.[17] and Fuller et al.[18] observed an increase in the carbonyl absorption with a simultaneous decrease in the C-H absorption region during weathering at 398° K and above. However, Martin and Chao found that during the weathering of Argonne Premium coal samples (73.0-85.6% C, maf) under ambient conditions the carbonyl absorption increases while the C-H absorption

in the aliphatic region remains unaffected[19]. Liotta et al. found that the concentrations of ether and carboxylic acid groups increase upon prolonged ambient temperature weathering of Illinois #6 coal[16]. Painter et al. also have noted formation of carbonyl and carboxylic acid groups with concurrent decrease in aliphatic C-H intensity during the initial stages of air oxidation of a highly caking Pennsylvania coal[17].

Our interest was to determine the fate of the aliphatic crosslinks during weathering. The aliphatic carbon structure, especially the crosslinks, play a significant role in coal liquefaction. The macromolecular network structure of bituminous and lower rank coals contains part of the aliphatic structure as methylene and polymethylene crosslinks connecting aromatic/hydroaromatic clusters. During liquefaction the relatively weak crosslinks undergo cleavage, while the hydroaromatic units provide part of the hydrogen for capping the free radicals produced by thermal decomposition[1]. Therefore, the changes in aliphatic carbon distribution in coal during weathering can influence its liquefaction behavior.
There are as yet no accurate methods available for quantifying the aliphatic crosslinks in coal. Quantitative nature of the application of infrared (IR) spectroscopy is limited to certain general types of functional groups or bond types. Nuclear magnetic resonance spectroscopy, despite the success of dipolar dephasing techniques to decipher the extent of substitution on carbon atoms, is still inadequate to distinguish distinct structural entities[20,21].

In our studies, we have used acid-catalyzed transalkylation of coal using phenol and boron trifluoride, first reported by Heredy and Neuworth[22], to quantify the aliphatic crosslinks in coals for monotoring changes in these crosslinks during weathering. It is assumed that during the transalkylation reaction, most of the methylene and polymethylene crosslinks are transferred to phenol. Since extensive solubilization is achieved by transalkylation, the information obtained from the analyses of the soluble products can provide useful information about coal structure. Although there are side reactions associated with the transalkylation reaction[23], we believe that it is adequate for comparing the relative features of raw and weathered coals. In addition to transalkylation, we have also used infrared studies to monitor the changes occurring during weathering.

EXPERIMENTAL

(a) Coal Samples. Three bituminous coals, namely, San Juan (New Mexico), Illinois #6, and Elkhorn (Kentucky) were used in the present study. Most of the studies were done on San Juan coal. The coals were collected from the freshly exposed mine faces. The samples were immediately transferred at the mine face to containers under a nitrogen atmosphere. The containeres were closed tightly, sealed, and stored at approximately 273° K. The grinding and sieving were done under a nitrogrn atmosphere. The ground and riffled samples were kept in glass jars, sealed under nitrogen, and stored in a refrigerator at 277° K. The proximate and ultimate analyses of the coal samples are given in Table 1.

(a) <u>Weathering of Coal Samples.</u> The coal samples, ground to -325 standard mesh, were subjected to accelerated weathering by heating them at 383° K in an air oven for 16 hours.

(c) <u>Transalkylation.</u> The procedure for transalkylation was essentially the same as that used by Heredy and Neuworth[22]. Briefly, coal(10 g) was slurried with phenol (100 g, Aldrich) in a three-necked round-bottomed flask equipped with a condenser and a thermometer, and heated to 373° K using a water bath. Boron trifluoride(Matheson) was bubbled through the coal-phenol slurry for 6 hours. The effluent gases were passed through saturated solution of sodium carbonate to neutralize the acids. At the end of 6 hours, BF_3 flow was stopped and the flask was purged with N_2 to remove any unreacted BF_3 and gaseous HF produced by the hydrolysis of BF_3. The reaction mixture, which now was a viscous suspension, was poured into 1 litre of ice-cold water. Sodium carbonate was added to the aqueous slurry with vigorous stirring until the aqueous layer was neutral. The neutralized reaction mixture was extracted successively with ether and toluene. Preliminary analyses by GC and HPLC indicated that the ether extract contained predominantly phenol and small quantities of coal-derived products. The toluene extract also contained phenol, but had a much larger proportion of coal-derived materials than the ether extract.

(d) <u>Analyses of the Reaction Products.</u> The ether and toluene extracts from the transalkylation reactions of fresh and weathered coals were analyzed by GC/MS on a VG-7070HS mass spectrometer in the EI mode. The mass spectrometer was interfaced with a Hewlett-Packard 5790 gas chromatograph. The GC column was a 35 meter long capillary with DB-1 as the stationary phase. A temperature program of 423-623° K at 8°/minute was used during the analysis. It was suspected that some of the high molecular weight phenolic compounds produced during the reaction may not be volatile enough for GC analysis. Therefore, the reaction mixture was silylated using N,O-bis trimethylsilylfluoroacetamide (BSTFA)[24] prior to analysis. Silylation of phenols converts them to silyl ethers, whose boiling points are considerably lower than those of the phenols. This procedure thus makes high molecular weight phenols more amenable to GC analysis. Bis-2 and bis-4 hydrohyphenyl methane were used as internal standards for quantification.

RESULTS AND DISCUSSION

Transalkylation involves the transfer of alkyl groups between aromatic nuclei, usually in the presence of strong Lewis acids. Heredy and Neuworth[22] used this reaction to "depolymerize" coal. As a result of the reaction of coal with BF_3 and phenol, the solubility of coal in phenol or pyridine increased substantially. Various modifications of this reaction have since been reported[25-28]. Transalkylation reactions in the presence of trifluoromethane sulfonic acid and aromatic hydrocarbons have recently been used by Benjamin et al.[27] and Farcasiu et al.[28] to identify structural features in coals and heavy petroleum ends, respectively.

It is believed that during transalkylation the aliphatic side chains and crosslinks transfer from coal, without rearrangement, to the aromatic substrate such as phenol or toluene. A typical reaction is depicted in Scheme I.
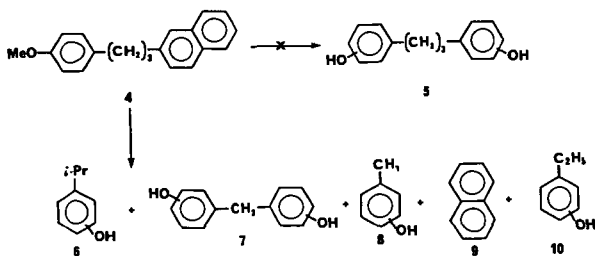
<u>Scheme I. Transalkylation</u>

Ar—CH₂—Ar $\xrightarrow[\text{BF}_3]{\text{Phenol}}$ HO—⬡—CH₂—⬡—OH + Ar—Ar

1   2   3
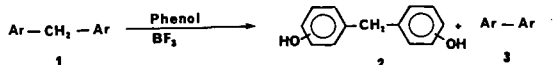
For the above reaction to occur, the aromatic nuclei in compound 1 should carry activating groups, such as hydroxyl, alkoxy, or fused ring aromatics[23,29]. As a result of reaction with BF_3 and phenol, the macromolecular structure of coal should undergo rupture at the aliphatic crosslinks, and these crosslinks are transferred to phenol molecules to produce bisphenols. Analysis of the bisphenols should provide information on the aliphatic crosslinks present in coal structure.

In model compounds, the aliphatic side chains on aromatic nuclei transalkylate without rearrangement[30,31]. However, the reaction of aliphatic crosslinks is more complicated. For example, transalkylation of 1-(4-methoxyphenyl)-3-(2-naphthyl) propane (Compound 4) under BF_3-phenol reaction conditions does not produce the expected 1,3-bishydroxyphenyl propane (Compound 5)[23]. Instead, it gives a variety of products resulting from the rearrangement and fragmentation of the trimethylene crosslink in Compound 4, as shown in Scheme II.

<u>Scheme II. Side Reactions During Transalkylation</u>

MeO—⬡—(CH₂)₃—⬢⬢ ——X——→ HO—⬡—(CH₂)₃—⬡—OH

4   5

i-Pr⬡OH + HO—⬡—CH₂—⬡—OH + CH₃⬡OH + ⬢⬢ + C₂H₅⬡OH

6   7   8   9   10

Because of the above considerations, it is not possible to determine the exact nature and concentration of of the crosslinks as they are present in coals by analysis of the transalkylation products. However, a comparison of the relative concentrations of the various crosslinks in different coal samples and how they change during weathering is possible. Specifically, our aim is to compare the relative concentrations of methylene and polymethylene crosslinks in fresh and weathered coals, so that the effect of weathering on these crosslinks can be assessed.

934

Numerous bisphenols of the general structure 11 were detected in both the ether and toluene extracts of the transalkylation products from the fresh and weathered coal samples.

11
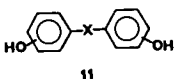
X = straight or branched chain aliphatic crosslink

Table 2 contains a list of the aliphatic crosslinks detected in the toluene extract. Compounds with methylene crosslinks were predominant in the products from the fresh coal. This is consistent with the results of Benjamin et al.[27]. It is interesting to note that several branched chain crosslinks appear in the transalkylation products from both the fresh and the weathered coals. Such crosslinks in coal structure have been reported only recently. Alkyl substituted methylene and ethylene crosslinks have been detectd in a Wyodak coal by Benjamin et al.[27]. In the present study, some of the branched chain crosslinks may have been formed by rearrangement of the straight chain crosslinks during transalkylation[23].

The relative concentrations of several types of hydrocarbon crosslinks, namely methylene($-CH_2-$), ethylene($-CH_2-CH_2-$), methyl methylene($-CH(CH_3)-$), methyl ethylene($-CH(CH_3)-CH_2-$), ethyl methylene($-CH(CH_2CH_3)-$), and propyl methylene($-CH(CH_2CH_2CH_3)-$) in the fresh and weathered San Juan coal are compared in Table 3. The concentrations are reported as a fraction of the toluene extract from the transalkylation reaction. As a result of weathering, concentrations of the most abundant, crosslinks namely, methylene, ethylene, methyl methylene, and ethyl methylene groups are reduced by factors of 6, 14, 6, and 9 respectively. The differences in the concentrations of larger crosslinks were not measured because of their low abundance in the transalkylated products.

The results in Table 3 clearly indicate that the aliphatic crosslinks have been altered significantly by oxidative weathering. The question is: what are these crosslinks converted to? Liotta et al. have detected, by infrared analysis, increases in carboxylic acid groups and ether linkages after long term ambient temperature weathering of an Illinois #6 coal[16]. Painter et al. have obtained infrared spectroscopic evidence for a decrease in the aliphatic stretching intensity (2900 cm^{-1} region) and an increase in the carbonyl stretching (1700-1765 cm^{-1} region) after weathering of a highly caking Pennsylvania coal[17,32]. They speculate the formation of ester groups, in addtion to ketones and carboxyl groups, as a result of extended weathering at about 373° K. Jakab et al. have reported that weathering of subbituminous coals causes changes in both the aliphatic and aromatic structures of coal[33]. They detected, by Curie Point pyrolysis GC-MS, an increase in carbonyl groups in the coals weathered in air at 373° K. In addition, they found decresed yields of alkylnaphthalenes and phenols from the weathered coal compared to the fresh coal. The decrease was attributed to condensation reactions involving alkyl aromatics and phenolic

935

fragments resulting in large clusters. Gethner has speculated that formation of ketones, aldehydes, esters, and ethers is likely during oxidative weathering of coals at 373° K[34]. Recently, Fuller has obtained high temperature infrared spectroscopic data which indicate that during oxidative weathering at 473° K or above[18], several surface groups such as ketones, aldehydes, carboxylic acids, and anhydrides of carboxylic acids are formed.

We have examined the infrared spectra of three coals before and after overnight weathering in air at 383° K. The infrared spectra of the fresh coals, their corresponding weathered samples, and the difference spectra between the weathered and fresh coals are given in Figures 1-3. Several changes due to weathering are observed. The most significant changes are the enhanced carbonyl absorptions in the 1700 cm^{-1} region, and decreases in the aliphatic C-H absorptions in the 2850-2950 cm^{-1} (CH stetching) and 1450 cm^{-1} (CH$_2$ bending) regions. These changes are quite discernible in the difference spectra. Minor changes are observed in the aromatic CH vibrations in the 750 - 850 cm^{-1} region as well, especially in the Elkhorn coal.

With regard to the results of our infrared study, a word of caution is appropriate. The large decreases in the concentration of the aliphatic crosslinks after weathering, as measured by transalkylation (Table 3), cannot be expected to match those indicated in the difference infrared spectra between weathered and fresh coals. This is because the spectra measure the total aliphatic content of the samples, namely aliphatic crosslinks, hydroaromatics, and aliphatic side chains. In contrast, results in Table 2 show differences in relative concentrations of the aliphatic crosslinks, which represent only a small part of the total aliphatics. Furthermore, concentrations measured by transalkylation correspond to only the soluble fractions of the reaction products; some of the more complex transalkylation products may be retained in the residue itself.

Our transalkylation studies show that the concentrations of methylene and other aliphatic crosslinks decrease during oxidative weathering. The infrared analysis shows that carbonyl groups are produced during weathering. Therefore, it is quite likely that during our weathering conditions the aliphatic crosslinks are oxidized to carbonyls and/or carboxylic acid groups.

A possible mechanism of oxidation of methylene groups to carbonyl groups involves autooxidation (oxidation by molecular oxygen) at the benzylic position. Autooxidation of arylalkanes is a facile reaction with low activation energies; for example, 6.0 kcal/mole for 1,1-diphenylethane and, 13.3 kcal/mole for toluene[35,36].

Auotoxidation of coals can be initiated by abstraction of a benzylic hydrogen atom by free radicals already present in coals[37-39]. The resulting benzylic radical then reacts with oxygen to form a peroxyradical, which abstracts a H-atom from elsewhere in the coal "molecule" to form a hydroperoxide. Formation of hydroperoxide during weathering is speculated by other workers as well[16,40,41]. The hydroperoxide can undergo homolysis at the peroxy bond (activation energy – 35 kcal/mole) to generate an alkoxy radical (Schemme III) which can undergo various reactions to produce carbonyl compounds. Some of the possible reactions of the alkoxy radical are represented in Schemes IV and V.

Scheme III.   Possible Oxidation Pathways

$$Ar-CH_2-Ar \xrightarrow[-RH]{R\cdot} Ar-\overset{\cdot}{C}H-Ar \xrightarrow{O_2} Ar-\underset{\underset{O-O\cdot}{|}}{C}H-Ar \xrightarrow[-R\cdot]{RH} Ar-\underset{\underset{O-O-H}{|}}{C}H-Ar$$

$$-ROH \downarrow R\cdot$$

$$Ar-\underset{\underset{O\cdot}{|}}{C}H-Ar$$

Scheme IV.   Possible Oxidation Pathways(contd.)

$$Ar-\underset{\underset{O\cdot}{|}}{C}H-Ar \xrightarrow[-R\cdot]{RH} Ar-\underset{\underset{OH}{|}}{C}H-Ar \xrightarrow[-RH]{R\cdot} Ar-\underset{\underset{OH}{|}}{\overset{\cdot}{C}}-Ar \xrightarrow[-RH]{R\cdot} Ar-\underset{\underset{O}{\|}}{C}-Ar$$

$$-RH \downarrow R\cdot$$

$$Ar-\underset{\underset{O}{\|}}{C}-Ar \qquad Ar-\underset{\underset{O}{|}}{C}H-Ar$$

$$Ar-\underset{}{C}H-Ar$$

Scheme V.   Possible Oxidation Pathways(contd.)

$$Ar-\underset{\underset{O\cdot}{|}}{C}H-CH_2-Ar \longrightarrow Ar-\underset{\underset{O}{\|}}{C}H \;+\; Ar-CH_2\cdot \longrightarrow \text{Various Products}$$

$$\longrightarrow Ar-COOH$$

$$-RH \downarrow R\cdot$$

$$Ar-\underset{\underset{O\cdot}{\|}}{C}-CH_2-Ar \longrightarrow Ar-CH-CH-Ar \longrightarrow Ar-\underset{\underset{O}{\|}}{C}-CH_2-Ar$$

937

There is ample evidence in the literature for conversion of reactive hydrocarbons to carbonyl compounds by autooxidation[42-48]. In coals, the final products of autooxidation under the conditions used in the present study could be a mixture of carbonyl and carboxylic acid surface groups. Under mild oxidation conditions, a different set of functional groups such as ethers as proposed by Liotta et al.[16] or epoxides as suggested in Scheme V could be formed. There are numerous examples of alkoxy radicals rearranging to epoxides[49-51]. Choi and Stock have shown that ethers can be produced from benzhydrol structures, which are invoked as intermediates in Scheme IV[52]. At higher temperatures, the epoxides and ethers are unstable and may rearrange to carbonyl compounds.

CONCLUSIONS

Oxidative weathering of coal causes a significant decrease in the concentration of aliphatic crosslinks; the relative decrease was determined by acid-catalyzed transalkylation of coal with phenol. Infrared analysis of the raw and weathered coals indicate that the hydrocarbon crosslinks are converted to carbonyl groups. Plausible explanations have been offered for the formation of carbonyl groups from aliphatic crosslinks.

ACKNOWLEDGEMENTS

REFERENCES

1. Buchanan, D, H., Warfel, L. C., Mai, W., and Lucas D. *Am. Chem. Soc.; Div. Fuel Chem., Preprints* 1987, 32(1), 146.
2. Neavel, R. C. Fuel 1976, 55, 237.
3. Chang, C. Y., Guin, J, A., and Tarrer, A. R. J. Chinese Chem. Soc. 1981, 28, 155.
4. Whitehurst, D. D., Mitchell, T. O., and Farcasiu, M. *Coal LIquefaction: the Chemistry and Technology of Thermal Process*, Academic Press, New York, 1980, page 112.
5. Senftle, J. T., and Davis, A. International Journal of Coal Geology 1984, 3, 375.
6. Meuzlaar, H. L. C., McClennen. W. H., Cady, C. C., metcalf, G. S., Windig, W., Thurgood, J. R., and Hill, G. R. *Am. Chem. Soc.; Div. Fuel Chem., Preprints* 1984, 29(5), 166.
7. Larsen, J. W., Lee, D., Shawver, S. E., and Schmidt, T. E. *GRI Annual Report, February 1984.*
8. Johnson, R. A., and Cooney, R. P. Aust. J. Chem. 1983, 36, 2549.
9. Orenbach, M. S. and Anchugova, N. A. Khim. Tverd. Topl. 1983, 2, 19.
10. Crelling, J. C., Schrader, R. H., and Benedict, L. G. Fuel 1979, 58, 542.

11. Sarkar, S. Fuel 1980, _59_, 450.
12. Vargha-Butler, E. I., Zubovits, T. K., Smith, R. P.,Tsim, I. H. L., Hamza, H. A., and Neuman, A. W. Colloids Surf. 1984, _8_, 231.
13. Wu, M. M., Robbins, G. A., Winschel, R. A., and Burke, F. P. _Am. Chem. Soc.,; Div. Fuel Chem., Preprints_ 1987, _32(1)_, 408.
14. Berkowitz, N. _Sample Selection, Aging, and Reactivity of Coal_, R. Klein and R. Wellek, Eds., Wiley-Interscience, New York, 1989, Chapter 5, pp 217-251.
15. Gray, R. J. and Lowenhaupt, D. E. _Sample Selection, Aging, and Reactivity of Coal_, R. Klein and R. Wellek, Eds., Wiley-Interscience, New York, 1989, Chapter 6, pp 255-334.
16. Liotta, R., Brons, G., and Isaacs, J. Fuel 1983, _62_, 781.
17. Painter, P. C., Coleman, M. M., Snyder, R. W., Mahajan, O. P., Komatsu, M., and Walker, P. L., Jr. Applied Spectroscopy 1981, _35_, 106.
18. Fuller, E. L.,Jr. and Smyrl, N. R. _Am. Chem. Soc.; Div. Fuel Chem., Preprints_ 1988, _33(4)_, 691.
19. Martin, K. A. and Chao, S. C. _Am. Chem. Soc.; Div. Fuel Chem., Preprints_ 1988, _33(3)_, 136.
20. Pugmire, R. J., Woolfenden, W. R., Mayne, C. L., Karas, J., and Grant, D. M. _Am. Chem. Soc.; Div. Fuel Chem., Preprints_ 1983, _28(1)_, 103.
21. Murphy, P. D., Cassidy, T. J., and Gerstein, B. C. Fuel 1982, _61_, 1233.
22. Heredy, L. A. and Neuworth, M. B. Fuel 1962, _41_, 221.
23. Joseph, J. T. and Mahajan, O. P. Fuel, 1985, _64_, 1321.
24. Stalling, D. L., Gehrke, C. W., and Zumwalt, R. W. Biochem. Biophys. Res. Comm. 1968, _31_, 161.
25. Ouchi, K., Imuta, K., and Yamashita, Y. Fuel 1965, _44_, 29.
26. Yurum, Y. and Yiginsu, I. Fuel 1981, _60_, 1027.
27. Benjamin, B. M., Douglas, G. C., and Cannonico, D. M. Fuel 1984, _63_, 888.
28. Farcasiu, M., Forbus, T. R., and La Pierre, R. B. _Am. Chem. Soc.; Div. Pet. Chem., Preprints_ 1983, _28(2)_, 279.
29. Larsen, J. W. and Lee, D. Fuel 1983, _62_, 918.
30. Heise, R. and Tohl, A. Justus Liebigs Ann. Chem. 1982, _270_, 155.
31. Bakoss, H. J., Roberts, R. M. G., and Sadri, A. R. J. Org. Chem. 1982, _47_, 4053.
32. Painter, P. C., Snyder, R. W., Pearson, D. E., and Kwong, J. Fuel 1980, _59_, 282.
33. Jakab, E., Windig, W., and Meuzlaar, H. L. C. Energy and Fuels 1987, _1_, 161.
34. Gethner, J. S. Fuel 1985, _64_, 1443.
35. Gaddelle, C. and Clement, G. Bull. Soc. Chim. Fr. 1968, #1, 44.
36. Lloyd, W. G. _Methods in Free Radical Chemistry, Vol._ 4, E. S. Huyser, Ed., Marcel-Dekker, New York, 1973, Chapter 1, page 22.
37. Retkofsky, H. L., Hough, M. R., Maguire, M. M, and Clarkson, R. B. _Coal Structure_, M. L. Gorbaty and K. Ouchi, Eds.; Am. Chem. Soc. Symposium Series #192, 1981, Chapter 4.
38. Petrakis, L, Grandy, D. W., and Jones, R. B. Fuel 1982, _61_, 21.
39. Dack, S. W., Hobday, M. D., Smith, T. D., and Pilbrow, J. R. Fuel 1984, _63_, 39.
40. deVries, H. A. W., Bokhoven, C., and Dormans, H. H. Brennst. Chem. 1959, _50_, 289.
41. Lynch, B. M., Lancaster, L., and MacPhee, J. A. _Am. Chem. Soc.; Div. Fuel Chem., Preprints_ 1987, _32(1)_, 138.
42. Benson, S. W. J. Chem. Phys. 1961, _34_, 521.
43. Nangia, P. and Benson, S. W. J. Am. Chem. Soc. 1964, _86_, 2770.

44. Jones, J, H., Allendorf, H. D., Hutton, D. W., and Fenske, M. R. J. Chem. Eng., Data 1961, *6*, 620.
45. Fish, A. Proc. Roy. Soc. (London) 1966, *A293*, 378.
46. Fish, A. Proc. Roy. Soc. (London) 1967, *A298*, 204.
47. Zeelenberg, A. P., and Bickel, A. F., J. Chem. Soc. 1961, 4014.
48. Russel, G. A. J. Am. Chem. Soc. 1979, *79*, 3871.
49. Fish, A., Haskell, W. W., and Read, I. A. Proc. Roy. Soc. (London) 1969, *313*, 261.
50. Shaw, R. and Trotman-Dickenson, A. F. J. Chem. Soc. 1960, 3210.
51. Trimm. D. L. and Cullis, C. F., J. Chem. Soc. 1963, 1430.
52. Choi. C. Y. and Stock, L. M. J. Org. Chem. 1984, *49*, 2871.

TABLE I. Proximate and Ultimate Analyses of Coals

Proximate Analysis (wt %, dry basis)	San Juan	Ill #6	Elkhorn
Ash	11.4	11.8	6.6
Volatile Matter	44.2	39.7	38.7
Fixed Carbon	44.4	48.5	54.8

Ultimate Analysis (wt %, dmmf*)			
Carbon	78.9	78.9	85.4
Hydrogen	6.0	5.4	5.7
Nitrogen	1.6	1.2	1.8
Chlorine	0.1	0.1	0.2
Sulfur	1.0	4.4	0.7
Oxygen (by diff.)	12.4	10.0	6.3

*Dry, mineral matter-free basis

TABLE II. Crosslinks Detected in the Transalkylated Products

Crosslink	Formula
Methylene	$-CH_2-$
Ethylene	$-CH_2-CH_2-$
Mehtylmethylene	$-CH(CH_3)-$
Ethylmethylene	$-CH(CH_2CH_3)-$
Propyl methylene	$-CH(CH_2CH_2CH_3)-$
Methylethylene	$-CH(CH_3)-CH_2-$
Ethylethylene	$-CH(CH_2CH_3)-CH_2-$
Butylmethylene	$-CH(CH_2CH_2CH_2CH_3)-$

TABLE III. <u>Relative Concentrations of Crosslinks in the Transalkylated Products
from Fresh and Weathered San Juan Coal.</u>

Crosslink	Relative Concentration Fresh	Weathered	Ratio: Fresh/Weathered
$-CH_2-$	5.16	0.85	6
$-CH_2-CH_2-$	1.8	0.13	14
$-CH(CH_3)-$	1.08	0.17	6
$-CH(CH_3)-CH_2-$	1.04	0.11	9
$-CH(CH_2CH_3)-$	0.67	0.09	7
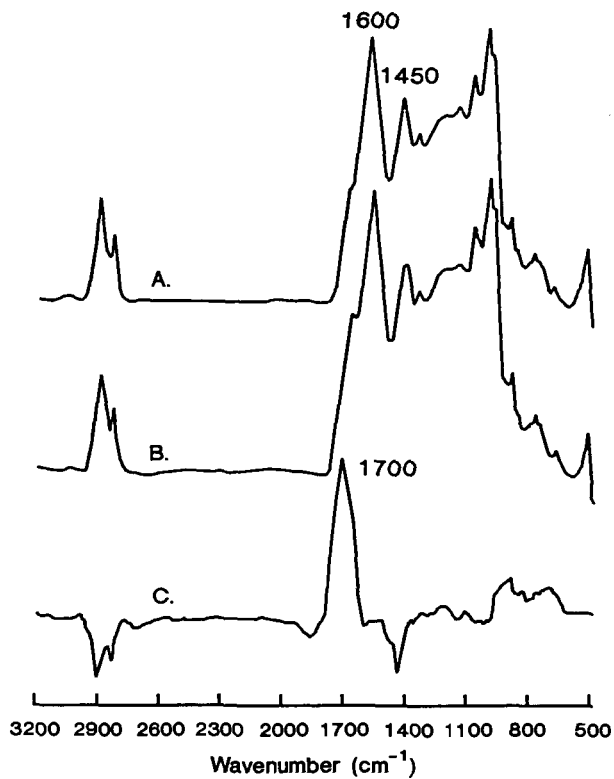
Figure 1. Infrared spectra of San Juan coal

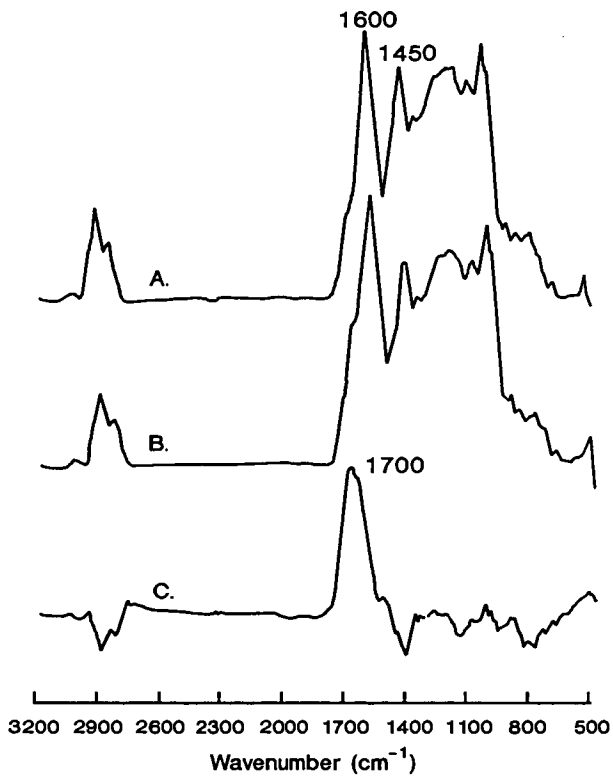A. Fresh coal, B. Weathered coal, and C. Difference spectrum (B–A).

943

Figure 2. Infrared spectra of Illinois #6 coal
A. Fresh coal, B. Weathered coal, and C. Difference spectrum (B–A).
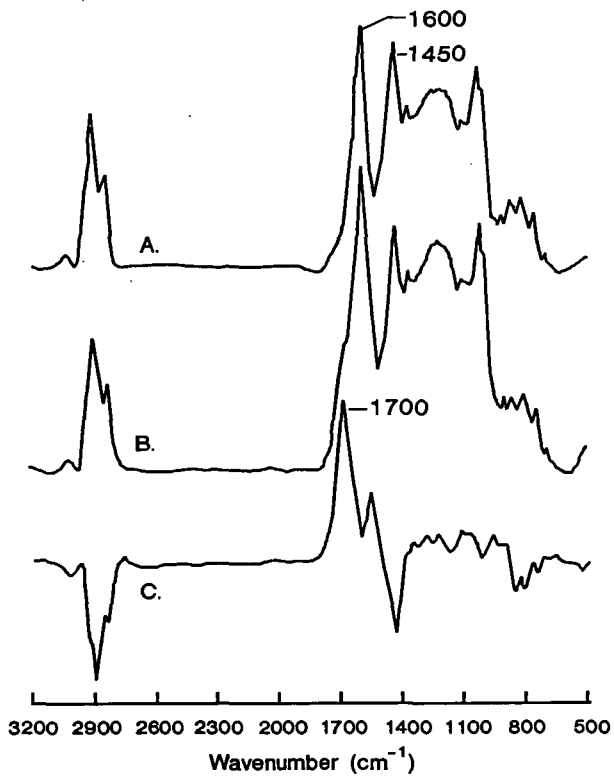
Figure 3. Infrared spectra of Elkhorn coal
A. Fresh coal, B. Weathered coal, and C. Difference
spectrum (B-A).